DURABILITY TESTING AND VIBRATION CHARACTERIZATION OF AN ELECTRIC VEHICLE BATTERY

A Thesis

by

Halil Zınar DÜZGÜN

Submitted to the
Graduate School of Sciences and Engineering
In Partial Fulfillment of the Requirements for
the Degree of

Master of Science

in the
Department of Mechanical Engineering

Özyeğin University
April 2022

DURABILITY TESTING AND VIBRATION CHARACTERIZATION OF AN ELECTRIC VEHICLE BATTERY

Approved by:

Assistant Professor Polat Şendur, Advisor
Department of Mechanical Engineering
Özyeğin University

Assistant Professor Ramazan Ünal
Department of Mechanical Engineering
Özyeğin University

Associate Professor Ali Çınar
Department of Mechanical Engineering
MEF University

Date Approved: 26 April 2022

To my family...

ABSTRACT

Although the electrical system is important in the development of electric vehicles, the durability of the battery against mechanical loads and the performance of the battery against shock reactions are just as important. The objective of this study is to investigate the structural life of the battery of the C-platform sports utility vehicle (SUV). For this purpose, a power spectral density (PSD) durability test profile is generated and compared to battery test standards such as ISO 6469:2019, AK-LH 5.21 and SAE J2380. Analytical Virtual Proving Ground (VPG), a multibody dynamics simulation model, is also developed and correlated to test data. The results show that fatigue damage spectrum (FDS) values for AK-LH is higher than the fatigue damage of the collected vehicle data, while the FDS results for ISO standard are lower compared to the vehicle data. The results also indicate that the loads in the longitudinal (x-direction) and lateral (y-direction) directions are different, and therefore loads with different amplitudes should be used for these directions. Finally, it is concluded that the VPG model can be used for determining the fatigue life when there is no test data, thanks to its high accuracy.

ÖZETÇE

Elektrikli araçların geliştirilmesinde elektrik sistemi çok önemli olsa da bataryanın mekanik yüklere karşı dayanıklılığı ve şok tepkilerine karşı performansı da bir o kadar önemlidir. Bu çalışmanın amacı, C-platformlu bir aracın (SUV) bataryasının yapısal ömrünü araştırmaktır. Bu amaçla, bir spectral güç yoğunluğu (PSD) dayanıklılık test profili oluşturulup, ISO 6469:2019, AK-LH 5.21 ve SAE J2380 gibi pil test standartlarıyla karşılaştırılmıştır. Çoklu cisim dinamiği simülasyon modeli olan Sanal Test Pisti (VPG) de geliştirilmiş ve test verileriyle karşılaştırılmıştır. Sonuçlar, AK-LH için spectral yorulma hasar (FDS) değerlerinin toplanan araç verilerinin yorulma hasarından daha yüksek olduğunu, ISO standardı için FDS sonuçlarının ise araç verilerine göre daha düşük olduğunu göstermektedir. Sonuçlar ayrıca boyuna (x-yönü) ve yanal (y-yönü) yönlerdeki yüklerin farklı olduğunu ve dolayısıyla bu yönler için farklı genliklere sahip yüklerin kullanılması gerektiğini göstermektedir. Son olarak, VPG modelinin yüksek doğruluğu sayesinde test verilerinin olmadığı durumlarda yorulma ömür verilerini belirlemek için kullanılabileceği sonucuna varılmıştır.

ACKNOWLEDGEMENTS

First of all, I would like to thank to my beloved family for their support in life, in work and in my study. They have been always there to encourage me.

It was a great pleasure and honour for me to work with my advisor Dr. Şendur on my M.Sc study. I'm deeply indebted to Dr. Şendur for his kind support. It was a privilege for me to be under his lights on the way of my study, project and thesis.

Last but not least, I would like to thank to my co-workers and managers in Turkey and my colleagues in UK. It was a team work to be able to write this thesis.

TABLE OF CONTENTS

DEDICATION . . . . . **iii**

ABSTRACT . . . . . **iv**

ÖZETÇE . . . . . **v**

ACKNOWLEDGEMENTS . . . . . **vi**

LIST OF TABLES . . . . . **ix**

LIST OF FIGURES . . . . . **x**

I INTRODUCTION **1**

1.1 Literature Review 1

1.2 Objectives of the Thesis 4

II PSD PROFILE COMPARISON OF ELECTRIC VEHICLE BATTERY WITH STANDARDS **6**

2.1 Shock Response Spectrum, SRS 6

2.2 Extreme Response Spectrum, ERS 7

2.3 Fatigue Damage Spectrum Calculations 8

2.3.1 Rainflow Cycle Counting Method 8

2.3.2 Wöhler Curve and Fatigue Theory 10

2.3.3 Fatigue Damage Spectrum, FDS 11

2.4 Power Spectral Density (PSD) Test Synthesis 12

2.5 PSD Profile of Battery Electric Vehicle and Comparison with Standards 14

2.5.1 Physical Data Collection from Battery Electric Vehicle . . . 14

2.5.2 Test Standards 18

2.5.3 Results 19

III ANALYTICAL VEHICLE MODEL AND DATA **24**

3.1 Analytical Vehicle Model 24

3.1.1 Vehicle Modeling 25

3.1.1.1 Template 25

3.1.1.2 Subsystem 26

3.1.1.3 Assembly 27
3.1.1.4 Rigid and Flex Bodies 28
3.1.1.5 Vehicle Model 30
3.1.2 Tire Model 32
3.1.3 Road Model 33
3.2 Correlation and Results 35
IV CONCLUSION 38
V FUTURE WORK 39
REFERENCES 40
VITA 44

LIST OF TABLES

1 ISO 6469:2019 (12 hours per direction) 19
2 AK-LH 5.21 cycle (40 hours per direction) 19

LIST OF FIGURES

1 Passenger Car Battery (Pack) [2], [3]. 1

2 Details of Battery [4] 2

3 Base acceleration of the SDOF system 7

4 Rainflow cycle counting (a) force as a function of time, (b) the loading history[31] 9

5 Example of S-N Curve[35] 10

6 Probability of in-service failure[26] 12

7 PSD calculation schema 14

8 Resonance Road Surface [39] 15

9 Pave Road Surface [39] 15

10 Resonance Road Z Axis Data for left and right accelerometers . . . 16

11 Pave Road Z Axis Data for left and right accelerometers 16

12 Comparison of lifetime mileage (km) distribution between petrol and diesel passenger cars (2012-2013) [40] 17

13 Average lifetime mileages from 2006-2013 for passenger car [40] . . 18

14 FDS Comparison of ISO, AK-LH and collected data in X-axis . . . 20

15 FDS Comparison of ISO, AK-LH and collected data in Y-axis . . . 20

16 FDS Comparison of ISO, AK-LH and collected data in Z-axiss . . . 21

17 PSD Comparison of ISO and collected data in X-axis 22

18 PSD Comparison of ISO and collected data in Y-axis 23

19 PSD Comparison of ISO and collected data in Z-axis 23

20 Vehicle, tire and road [48] models 25

21 Template example of multilink suspension from Adams shared library 26

22 Subsystem example of multilink suspension from Adams shared library 27

23 Assembly example of a vehicle model from Adams shared library . . 28

24 Flexible body of the used vehicle model 30

25 Bushing force at lower control arm 31

26 The FEA model of the battery 32

27 Full vehicle model used in VPG Simulations 32

28 Pressure profile of the Ftire model on Belgian block road [51] 33
29 Concept of the OpenCRG road model [45] 34
30 Pave road example from Idiada Proving Ground [52] 34
31 Pave road example from Mira Proving Ground [53] 35
32 FDS Comparison of VPG and collected data in X-axis 36
33 FDS Comparison of VPG and collected data in Y-axis 37
34 FDS Comparison of VPG and collected data in Z-axis 37

CHAPTER I

INTRODUCTION

1.1 Literature Review

Renewable energy has increased its importance more recently with the increasing environmental awareness. Electric and hybrid electric vehicles have become more common every day following further demands of greenhouse gas emissions and pressure on exhaustion of natural resources [1]. Recently there has been increasing research activity on hybrid electric vehicles due to their attractive fuel economy and emission characteristics in the automotive industry. Along with the widespread use of electric vehicles (EVs), many different technical problems have become a research topic. These topics include battery systems, range, vehicle mitigation, safety and information technology and gear noise. Although hybrid and electric vehicles have made great progress in the last 20 years, the market is still very small compared to fossil fuel vehicles due to high cost, low range and charging times. The most important ingredient affecting these factors is the batteries of these vehicles.

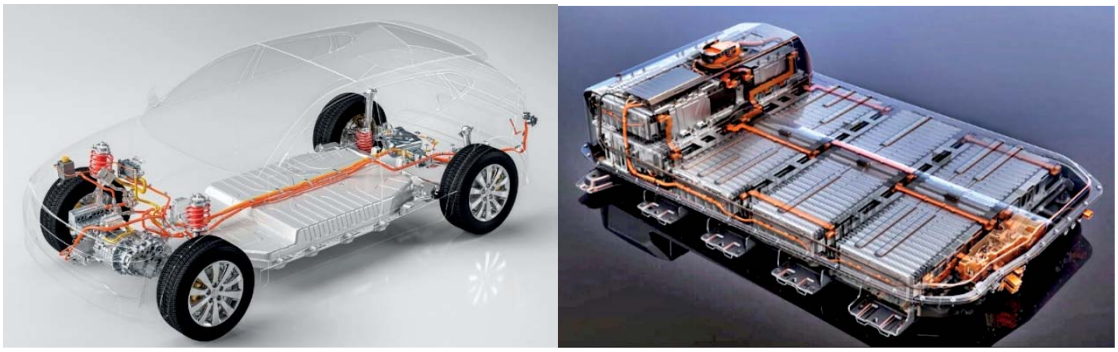

Figure 1: Passenger Car Battery (Pack) [2], [3].

Electrical vehicle batteries are not different from the batteries currently used in our phones or computers in that they are packaged parallel or sequentially. The

smallest element of the batteries is called a “cell” and meets the energy needs of vehicles. Modules are created by combining the cells, shown in Figure 2. Finally, battery packs are made up of modules [4].

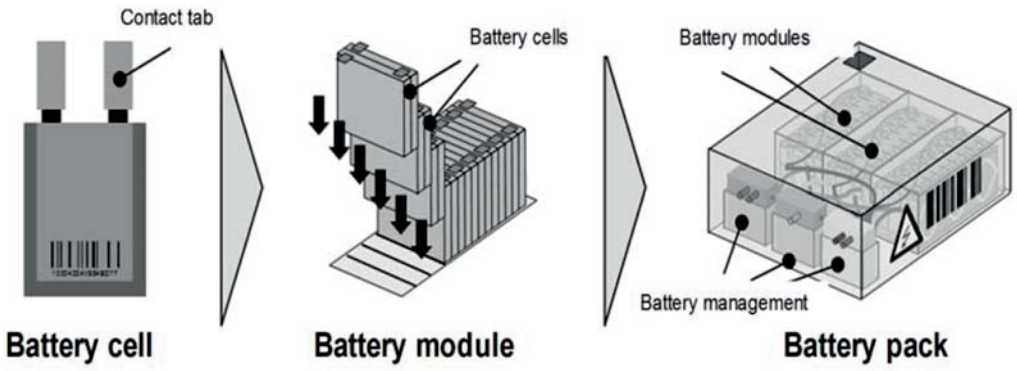

Figure 2: Details of Battery [4]

Battery pack is one of the costliest components of an electric vehicle [5]. The durability of batteries is of great importance due to their raw materials (especially lithium) and their complex structure. In most cases, batteries are placed under the vehicle due to the low center of gravity and better roll performance targets. The front and rear suspensions and the road impacts directly affect the structural life of the battery pack[6]. Therefore, although the electrical system is important in the development processes, the durability of the battery against mechanical loads and the performance of the battery against shock reactions are just as important.

In particular, ISO 12405-2 [7], ISO 6469-1 [8], AK-LH 5.21 [9] and SAE J2380 [10] standards refer to vibration-based tests and indicating the shock resistance and durability tests of the battery packs. In these tests, mechanical shaker tables or multi-axis shaker tables (MAST) are commonly used. The studies on the mechanical strength of the batteries are limited in the literature. In these studies, measurements were made and evaluated from couple of EVs ([11], [12], [13], [14]). Besides, there are some studies available in the literature to evaluate the vibration

profiles for Smart Electric Drive (ED), Nissan Leaf and Mitsubishi i-MiEV vehicles ([11],[13],[14],[15]). These vehicles are compact city vehicles and standards must cover wide range of vehicle segments. Especially road induced loads vary from vehicle segment to segment, and parameters like suspension kinematics, suspension parameters, vehicle mass and center of gravity have direct effect on the durability loads. In most of the studies in the literature, the data collected from the vehicles were calculated based on 100K miles (approximately 161K km) and 10 years of life ([11],[13],[14]). However, automobile OEMs can carry out tests according to quality standards for more than 100K miles to be more competitive in the vehicle market. Therefore, the standards must meet the expectations of these requirements. Therefore, the number of subjects in the focus group should be increased. In addition, the test data should be calculated with higher mileage and compared with the standards.

As can be seen from the aforementioned studies, data collection studies were mostly carried out at Millbrook proving ground ([11],[13],[14],[15]). There are many test tracks, where road profiles are designed from customer and field testing, in the world. While customer correlation studies are carried out on test tracks, different calculation methods such as level crossing, rainflow cycle count, relative damage spectrum (RDS), fatigue damage spectrum (FDS) and pseudo damage indices are used to optimize the cycles of the test track according to the durability life requirement of the target customer[16]. Customer correlation studies are carried out simultaneously by using test data collected from different locations on the vehicle ([17],[18]). These studies show that the fatigue life calculation methods and the sensor locations directly affect the fatigue life. It is also known that the test data collected from different markets can change the loads in the life calculation and correlation study [17]. Considering all these studies, it can be concluded that the life and shock calculations for the battery system will differ according to parameters such as the vehicle variant and the vehicle market.

Despite all these differences between standards, quite interesting results are encountered in the literature. For example, SAE J2380 [10] and USABC [19] standards state that the fatigue test should be performed with loads of the same magnitude in the longitudinal and lateral directions. On the contrary, different studies show that vehicles are subjected to different loads in these directions, which should be considered in determining the fatigue life of batteries ([11],[20]).

Another important observation from the literature is related to the frequency ranges in which durability tests are performed. SAE J2380 [10] and BS IEC 62660-2 [21] standards specify tests to be performed at 10 Hz and above, while ISO 12405-2 [7]uses a test profile starting at 5 Hz. Kjell and Lang highlight the importance of fatigue loads below 10Hz in a Volvo C30 electric vehicle [12]. Similarly, high magnitudes of durability load below 5 Hz in the cylindrical cells of the Smart Vehicle [15] are presented in another study. The shaker tables can provide excitations starting from 5 Hz as an important consideration in testing ([13],[14]).

1.2 Objectives of the Thesis

There are many parameters that affect the durability performance of any component in a vehicle. The location on the vehicle, the load capacity of the part, the suspension type, vehicle weight and center of gravity are among the most important parameters. All these variations play an important role in the fatigue loads imposed on a component. In order to have an efficient and competitive vehicle in the market, system, subsystem and component level tests should be performed according to realistic fatigue loads. In addition, the durability life of any component also depends on the user profile of the vehicle market and OEM's quality standards. Studies in the literature show that the type of the vehicle directly affects the vibration characteristics of the battery ([11],[12],[13],[14]). The objective of this study is to determine the structural life of the battery from road excitations. For this purpose, road load data is collected from a Turkish original

equipment manufacturers (OEMs) electric vehicle on different roads in a global proving ground in England. In this study, the test profile for the longitudinal, lateral and vertical directions will be examined for a fatigue life target of more than 100K miles. A power spectral density (PSD) durability test profile is created and compared to battery test standards such as ISO 6469:2019 [8] and AK-LH 5.21 [9]. Analytical Virtual Proving Ground (VPG), a multibody dynamics simulation model, is also developed and correlated to test data.

The remainder of this thesis is organized as follows. First, the PSD generation algorithms are explained. Then, the details concerning the experimental data collection and test results are provided. Subsequently, VPG model, a multibody dynamics-based simulation model is revealed. The correlation results between the VPG model and the experimental data are presented. Finally, the main conclusions of the paper are summarized.

CHAPTER II

PSD PROFILE COMPARISON OF ELECTRIC VEHICLE BATTERY WITH STANDARDS

In this chapter, the PSD profiles of electric vehicle batteries are compared with various engineering standards. Shock Response Spectrum (SRS) is described in Section 2.1. Extreme Response Spectrum (ERS) and Fatigue Damage Spectrum Calculations are explained in Section 2.2 and Section 2.3, respectively. Power Spectral Density (PSD) test synthesis is demonstrated in Section 2.4. The PSD profiles of battery electric vehicles are compared with engineering standards in Section 2.5. Results are discussed in Section 2.6.

2.1 Shock Response Spectrum, SRS

Shock response spectrum (SRS) is used to evaluate the earthquake loads in buildings with single degree of freedom (SDOF) response[22], shown in Figure 3. It has also proven useful in component response analysis for SDOF systems [23]. The dynamic response of a system is amplified when excited close to the natural frequency of the system, where the response highly depends on the damping of the system ([24],[25],[26]). SRS is used for the systems with unknown natural frequencies to calculate the maximum response in the vibration spectrum in the frequency range of interest [22]. The maximum response of the system for each frequency band is represented in the spectrum, which is called shock response spectrum (SRS). The maximum response of the dynamic system is directly dependent on the damping of the system, and structural damping is used as %5 commonly in the literature ([24],[25],[26]). Since the strain energy is proportional to the displacement rather than acceleration, the displacement is more representative of the failure mechanism [25].

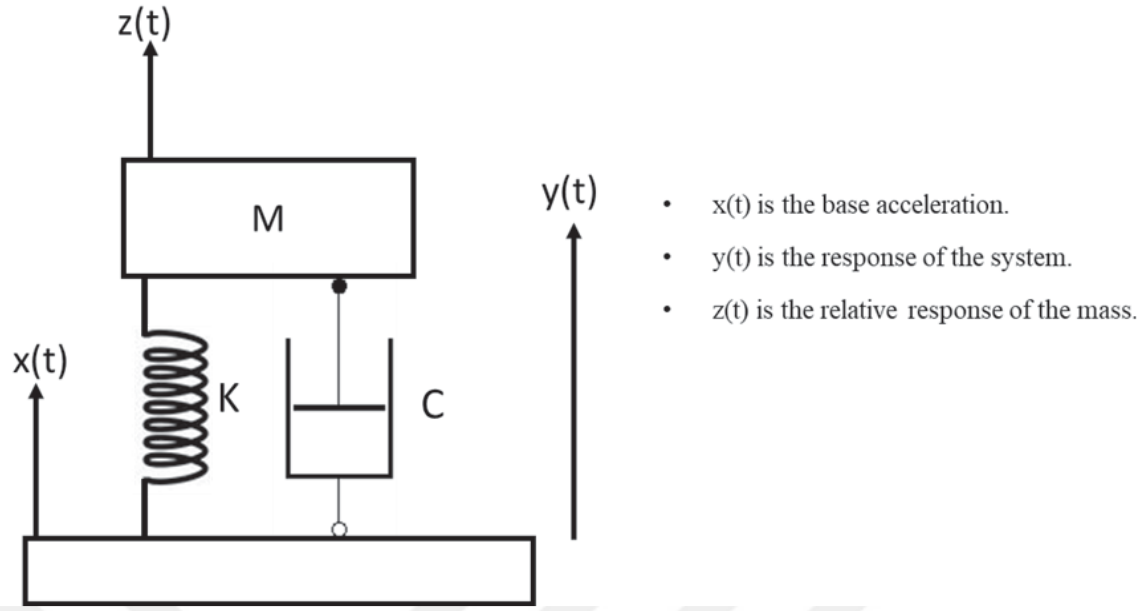

Figure 3: Base acceleration of the SDOF system

2.2 Extreme Response Spectrum, ERS

Extreme response spectrum (ERS) is also used to calculate the maximum response in a SDOF system. The SRS can be determined from the random acceleration signal, while the ERS can be calculated from the power spectral density. Miles [27] derived an expression for calculation of ERS ([24],[25],[26]). Lalanne [28] modified the Miles equation with Rayleigh probability function, as shown in Equation (1), to calculate the maxi-max response spectrum (MRS) ([24],[25],[26]). The maximum response for displacement for an SDOF system can be calculated according to Equation (2) ([24],[25],[26]).

$$ERS_{acc}(f_n) = \sqrt{\pi.f_n.Q.G_z(f_n).ln(f_n.T)} \tag{1}$$

$$ERS_{disp}(f_n) = \frac{ERS_{acc}(f_n)}{(2\pi.f_n)^2} \tag{2}$$

where $G_z(f_n)$ is the PSD excitation at frequency f_n, Q is the dynamic amplification factor and T is the PSD duration.

2.3 Fatigue Damage Spectrum Calculations

2.3.1 Rainflow Cycle Counting Method

The rainflow cycle counting method was developed by Endo and Matsuishi in 1968 [29]. Furthermore, Downing and Socie were verified the technique [30]and it became popular in the literature. Rainflow cycle counting algorithm is used to simplify random vibration as Sinusoidal vibrations. The name 'rainflow' is inspired from flow of rain from traditional Japanese structure Pagoda's roof edges.

For Endo and Matsuishi's rainflow count first random vibration signal needs to be rotated 90° to be able to represent Pagoda roof. Then, the following steps are followed:

1. A rain flow for each successive extremum point is considered.
2. A loading reversal is defined by allowing the flow from the roof until the followings are satisfied:
   (a) The drop is larger than maximum or smaller than the minimum at the opposite direction.
   (b) The flow follows previous flows from the above.
   (c) The rain is below the roof.
3. Each hysteresis cycle is determined by combining the same reversals[31].
4. Example of rainflow cycle count can be found in Figure 4.

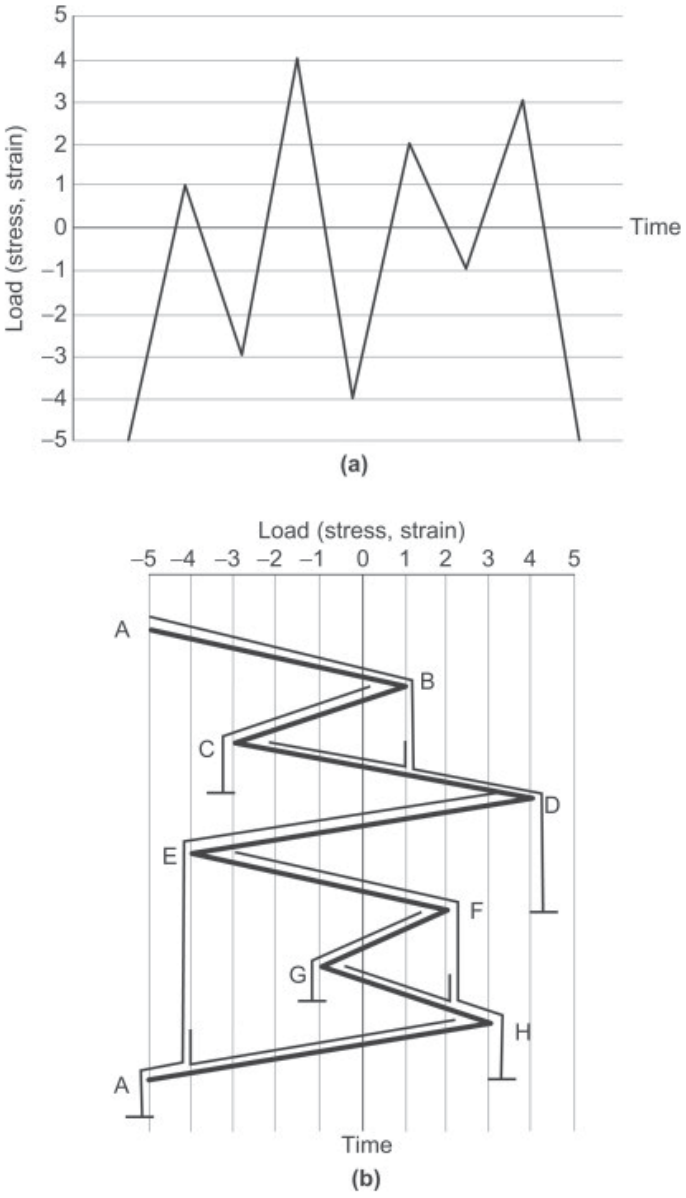

Figure 4: Rainflow cycle counting (a) force as a function of time, (b) the loading history[31]

2.3.2 Wöhler Curve and Fatigue Theory

Fatigue theory has a deep-rooted history in the industry [32]. However, the most important milestone is the work of railway engineer August Wöhler on train axles [32],[33]. Wöhler stated that the failure of parts operating under similar systematic loads at the end of a certain period is cyclical loads [33]. As a result of his studies, Wöhler showed that the strength of the components decreased because of the cyclic loads they are exposed to. After Wöhler's work Basquin introduced exponential law for demonstration of the fatigue with a stress-cyclic life (S-N) curve (also called Wöhler curve) with using Wöhler's test results example as shown in Figure 5 [34].

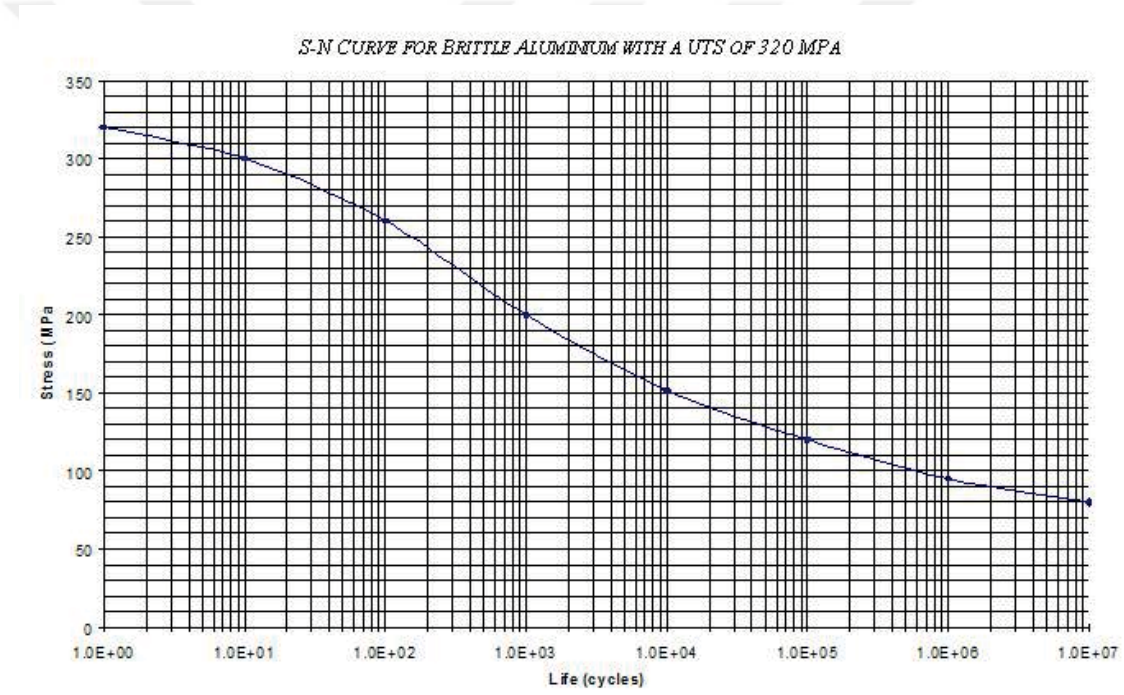

Figure 5: Example of S-N Curve[35]

Later on, in the fatigue theory Miner proposed cumulative fatigue damage calculation theory [36]. The theory is settled in our lives with the name of Miner's rule and it is basically based on calculating accumulated stresses with respect to their cycle numbers in the life estimation showed in Equation (3).

$$Damage = \sum_{i=0}^{k} \frac{n_i}{N_i} \tag{3}$$

Where k is the number of stress levels, n_i is the number of cycles at stress level i, and N_i is the fatigue life cycle at stress level i.

All these achievements on the fatigue theory brought us finite life estimation on material characterization study. In the industry in different types of work areas such as mining, energy, automotive etc. designed every component examined with respect to durability point of view.

2.3.3 Fatigue Damage Spectrum, FDS

Fatigue damage spectrum (FDS) is the frequency spectrum of the damage due to an excitation on a structure. It is used to evaluate the fatigue potential and to identify critical frequencies rather than as an absolute fatigue indicator. The FDS theory on the extreme response spectrum was suggested by Lalanne [37]. A similar approach of extreme response spectrum (ERS) was proposed in more recent studies ([24],[26]). FDS, the behavior of fatigue in terms of frequency, is explained with a simplest vibration model 'single degree of freedom (SDOF) system' natural frequencies with given damping ratio. To calculate fatigue damages collected random vibrations on any component can be used. The method is using the random vibration through base excitation of an SDOF system. Since stress is proportional to the displacement [38]. The relationship between the stress and the relative displacement, z(t), is shown in Equation (4) [26], [37]. Finally, the displacement data is processed with rainflow cycle counting method and fatigue damage is calculated from Equation (5) [26].

$$S = K_z(t) \tag{4}$$

$$N = \frac{C}{S^b} \tag{5}$$

Where S is stress, C is SN curve stress intercept, b is SN curve slope, N is fatigue life K is stiffness in the SDOF system.

2.4 Power Spectral Density (PSD) Test Synthesis

PSD is basically the Fourier transformation of a random signal in frequency domain. Fourier transformation is applied to measurements in time domain, and an average of the Fourier transformation is calculated for several signals [37]. Averages of the Fourier transformation represents the power spectral density (PSD).

While creating the fatigue test PSD profile, the safety factor should be calculated to eliminate the variations that may occur due to the environmental conditions and cycling in the measurements, as well as the tolerances on the strength of the material. The safety coefficient calculations can be made using Gaussian distribution or log-normal distribution. Log-normal distribution is given in Equation (6) [24].

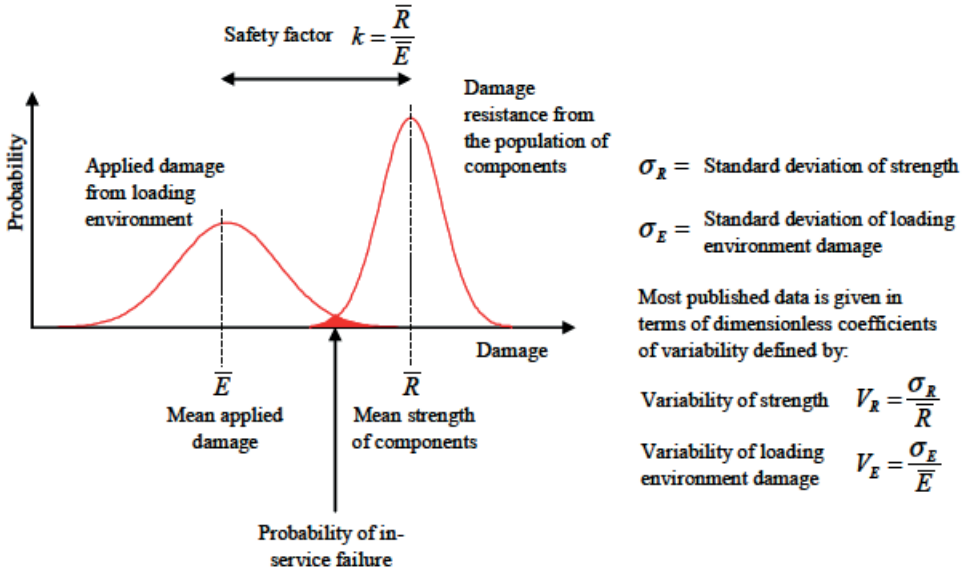

Figure 6: Probability of in-service failure[26]

$$k{=}exp\ \left\{ a^{'}.\sqrt{ln\left[\left(1{+}{V_R}^2\right).(1{+}{V_E}^2)\right]} - ln\left[\sqrt{\frac{1{+}V_E^2}{1{+}V_R^2}}\right]\right\} \tag{6}$$

Where a' is the probability of success (1-probability of failure) expressed as a number of standard deviation, V_R (variability of strength) and V_E (variability of loading enviroment damage) are dimensionless coefficients of variability, σ_R (strength)and σ_E (load environment damage) are standard deviations and E is mean applied damage and R is mean strength of components [24].

To create a PSD profile, the component life cycle should be assessed. A PSD profile should include the overall dynamic effects that the component will be subjected to over its lifetime. Durability structural tests are mostly done in proving grounds in the automotive industry. Proving grounds have a variety of road profiles and each road profile has a cycle number to excite the vehicle fatigue life based on customer usage. Measurements should be taken from all the road surfaces to create the PSD profile of the vehicle. FDS calculations are made for all roads in order to synthesize a PSD profile. Calculated FDS represents fatigue profile of the individual roads. The FDS value should be scaled with cycle number of roads to determine the overall fatigue life of the vehicle. Finally, scaled FDS values are added in order to assess the total fatigue damage on the component. Once total FDS is obtained, a PSD profile is then calculated using Equation (7):

$$\text{Vibration PSD } G(f_n) \ = \frac{2(2\pi.f_n)^3}{Q} \ .\left[\frac{k\sum FDS\ \ (f_n).C}{K^b.f_n.T.\Gamma\,(1{+}b/2)}\right]^{2/b} \tag{7}$$

$$\Gamma\,(g) = \int_0^\infty x^{(g-1)}.e^{-x}.dx \tag{8}$$

where $\sum FDS\ \ (f_n)$ is the total FDS.

The ERS of the calculated PSD profile should be compared with the SRS of the overall lifecycle. The SRS calculation for different road surfaces should be performed and the maximum envelope of the all the surfaces should be calculated to determine the maximum response to which the component is subjected. Since SRS is the maximum expected response of the component, calculated ERS of the PSD should not exceed the SRS of the component. The overall process flow for creating a PSD profile is shown in Figure 7.

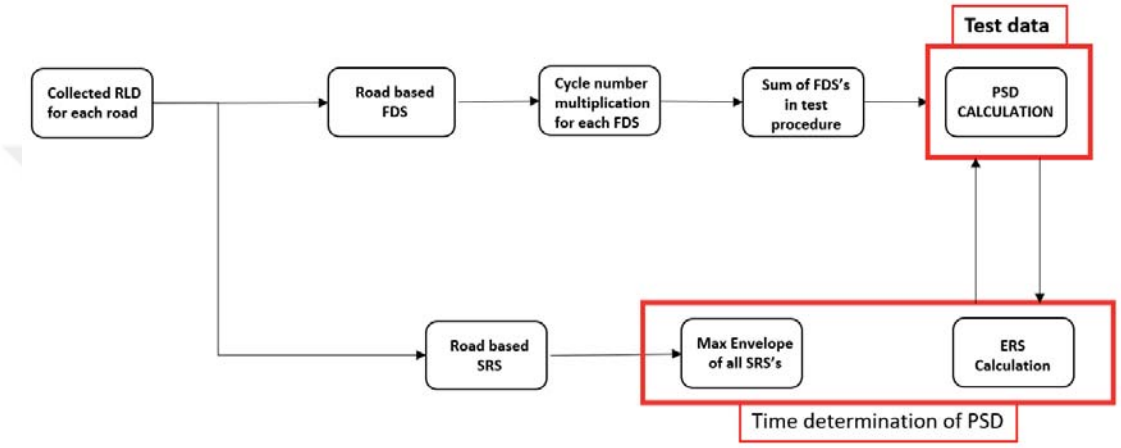

Figure 7: PSD calculation schema

2.5 PSD Profile of Battery Electric Vehicle and Comparison with Standards

2.5.1 Physical Data Collection from Battery Electric Vehicle

Road load data is collected from a prototype vehicle (C-platform SUV segment All Wheel Drive) of the Turkish OEM. Data is collected from a global proving ground in England. Proving ground structural durability procedure is used to evaluate the load profiles of the vehicle. Vehicle is loaded according to the test specifications and data is collected from various special durability road surfaces such as resonance road, shown in figure 8, and pave road, shown in Figure 9, at different speeds. Example of Z axis accelerations of battery can be seen in Figure 10 and 11.

Figure 8: Resonance Road Surface [39]

Figure 9: Pave Road Surface [39]

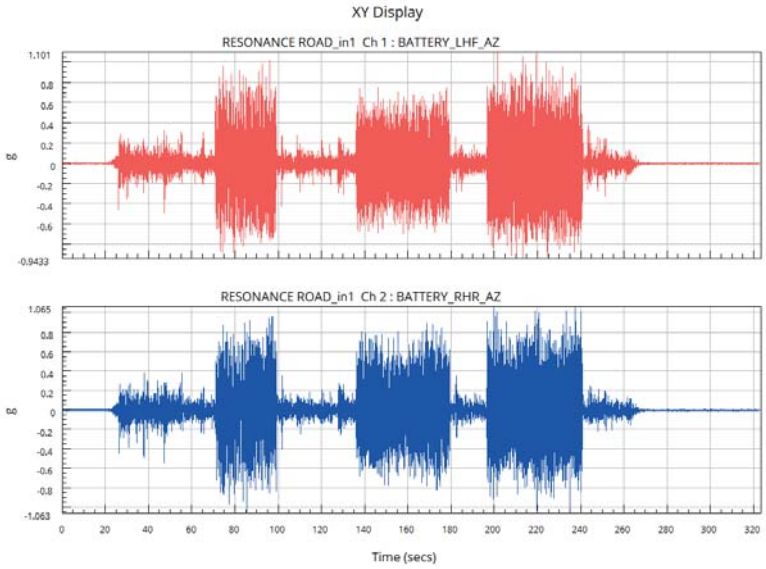

Figure 10: Resonance Road Z Axis Data for left and right accelerometers

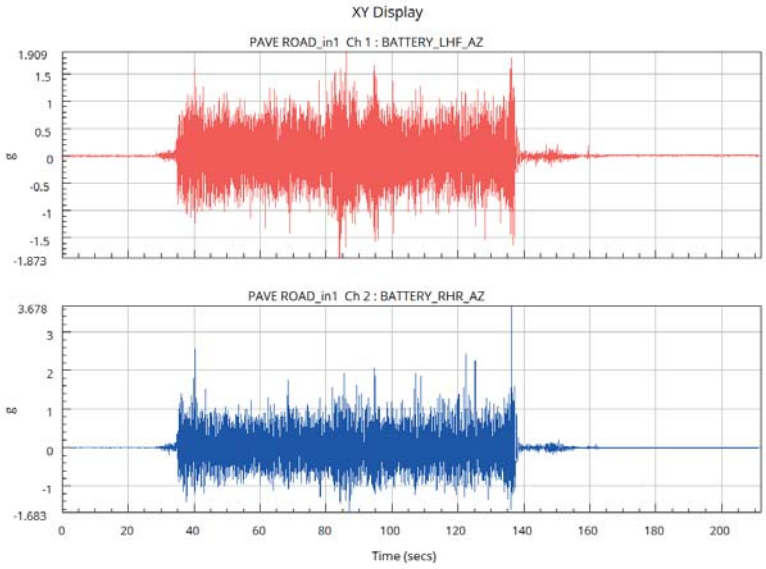

Figure 11: Pave Road Z Axis Data for left and right accelerometers

The durability lifetime depends on the annual driven mileage and the scrap age of the vehicle. The common durability lifetime is considered as between 200K km and 300K km in the literature [40],[41]. Therefore, calculated FDSs are evaluated for the 200K km and 300K km in this study. Yearly mileage information averages and distribution of the petrol and diesel passenger cars shown in Figures 12 and 13.

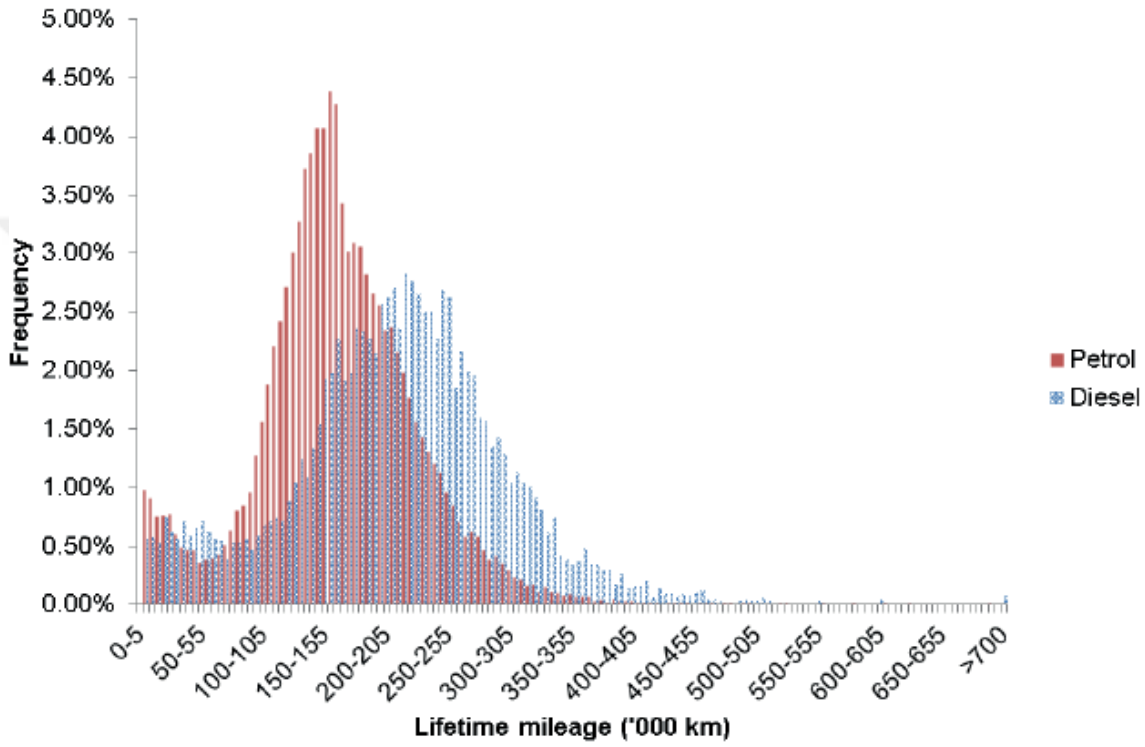

Figure 12: Comparison of lifetime mileage (km) distribution between petrol and diesel passenger cars (2012-2013) [40]

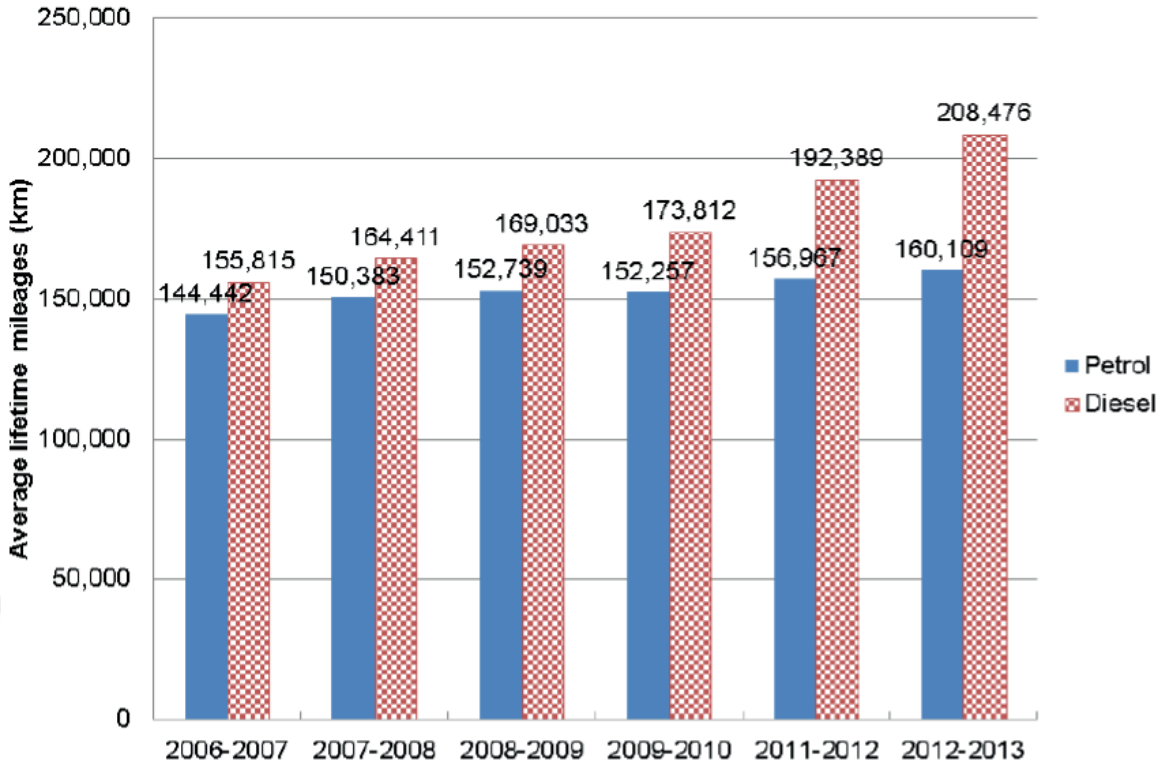

Figure 13: Average lifetime mileages from 2006-2013 for passenger car [40]

2.5.2 Test Standards

The PSD and FDS results are based on the most recent test standards, ISO 6469:2019 and AK-LH 5.21 in this study. The PSD profiles for ISO 6469:2019 and AK-LH 5.21 are given in Table 1 and Table 2, respectively. Since the profiles and durations for these standards are different, FDS results are calculated from PSD profiles to remove the time effect. The PSD profile generated using 12-hour experimental data is determined and compared to the ISO standard.

Table 1: ISO 6469:2019 (12 hours per direction)

PSD in X-direction		PSD in Y-direction		PSD in Z-direction	
Freq. (Hz)	PSD (g^2/Hz)	Freq (Hz)	PSD (g^2/Hz)	Freq (Hz)	PSD (g^2/Hz)
5	0.0003	5	0.002	5	0.0005
20	0.003	15	0.003	10	0.006
200	0.0000062	50	0.0003	15	0.004
		200	0.000004156	200	0.000004

Table 2: AK-LH 5.21 cycle (40 hours per direction)

PSD in X-direction		PSD in Y-direction		PSD in Z-direction	
Freq. (Hz)	PSD (g^2/Hz)	Freq (Hz)	PSD (g^2/Hz)	Freq (Hz)	PSD (g^2/Hz)
5	0.0029	5	0.0049	5	0.05100
8	0.0069	13	0.01866	9	0.04460
12	0.0127	50	0.00250	10	0.03850
16	0.0151			23	0.00680
22	0.0103			44	0.00230
50	0.0008			50	0.00183

2.5.3 Results

FDS results for ISO, AK-LH and collected data are compared in this section. FDS results are shown in Figure 14, Figure 15 and Figure 16 for x-axis, y-axis, and z-axis, respectively. The results show that FDS values for AK-LH is higher than the fatigue damage of the collected vehicle data, while the FDS results for ISO standard are lower compared to the vehicle data. The damage values from AK-LH are higher than test data for frequencies between 5 Hz to 50 Hz. In contrast, the damage values for ISO 6469 is lower at lower frequencies. It is an interesting observation that SAE J2380 [8] and USABC [17] are not closely correlated to the test data. The results show that the loads in the longitudinal (x-direction) and lateral (y-direction) are different, and therefore loads with different amplitudes should be used for these directions. The results also show significant fatigue loads between 5 Hz and 10 Hz, although SAE J2380 [8] and BS IEC 62660-2 [19] standards state that the testing should be performed above 10 Hz. These differences may lead to misleading conclusion about the fatigue life of the vehicle

components.

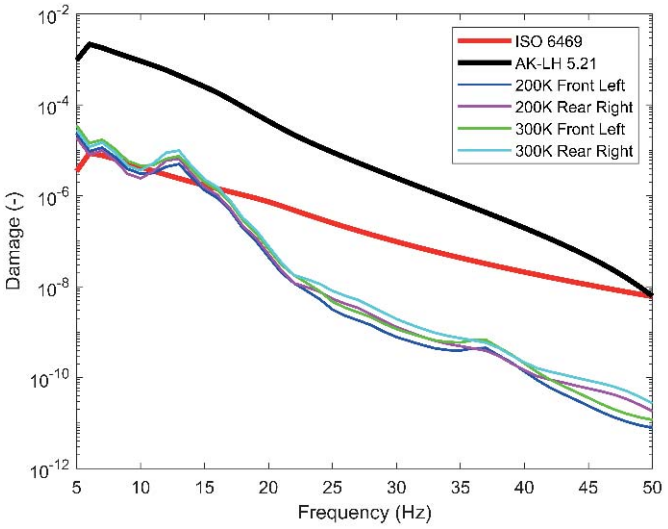

Figure 14: FDS Comparison of ISO, AK-LH and collected data in X-axis

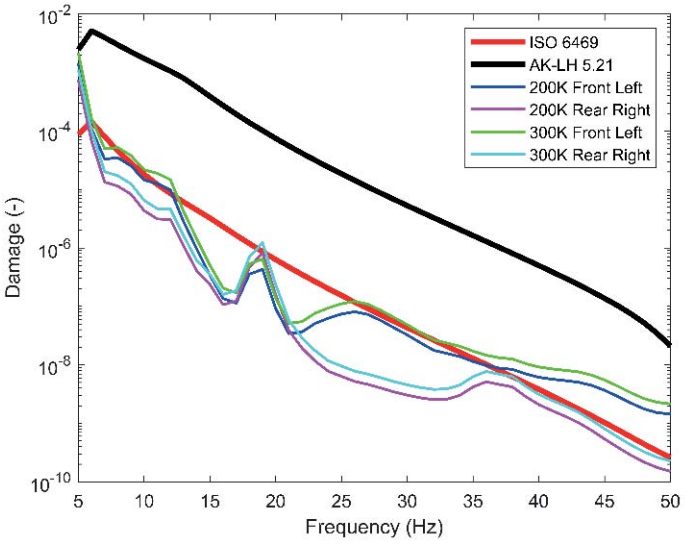

Figure 15: FDS Comparison of ISO, AK-LH and collected data in Y-axis

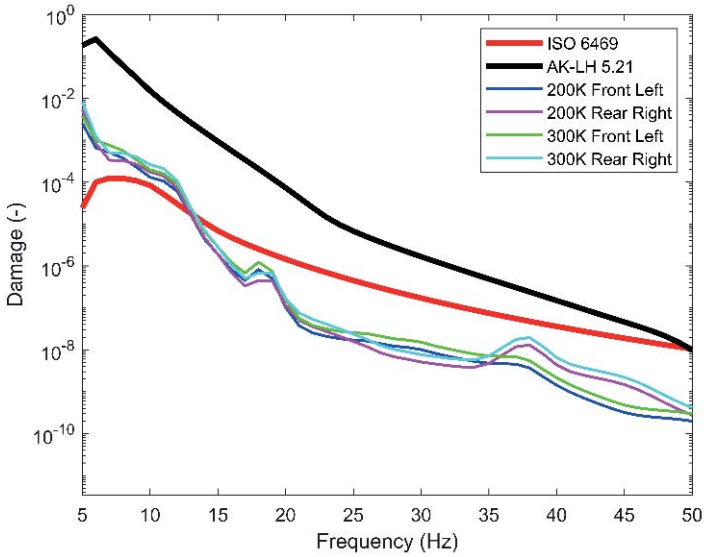

Figure 16: FDS Comparison of ISO, AK-LH and collected data in Z-axiss

The PSD parameters such as safety and test factors cause some variation with respect to the FDS results. Therefore, PSDs are calculated for 12 hours to compare with the ISO standard. Besides, the safety and test factors are taken as unity. The PSD results are shown in Figure 17, Figure 18, and Figure 19 for x, y, and z directions, respectively.

PSD comparison shows that ISO is more comparible with collected Vehicle data. This also shows that these factors is used while determining ISO standard. In PSD comparison ISO is lower in low frequencies but for frequencies higher then 15, ISO has higher amplitudes. There is a reactions at 37 Hz in Z direction in collected data which is higher than ISO is thought that non representative body movements caused this peak. In Y direction there are more peaks after 15 Hz higher than ISO. These behaviours suspected from physical Battery behaviour. Because normal batteries cover the underbody of the vehicles through side sills but prototype vehicle has small battery which does not covers all the underbody of the vehicle and this caused unexpected Y direction loads.

There is a linear approach to calculate 200K and 300K test procedures. This is also seen in comparisons. Sensor comparison of the Vehicle shows every sensors looks similar beside center acc Z axis due to distance from load points and damping during load transfer.

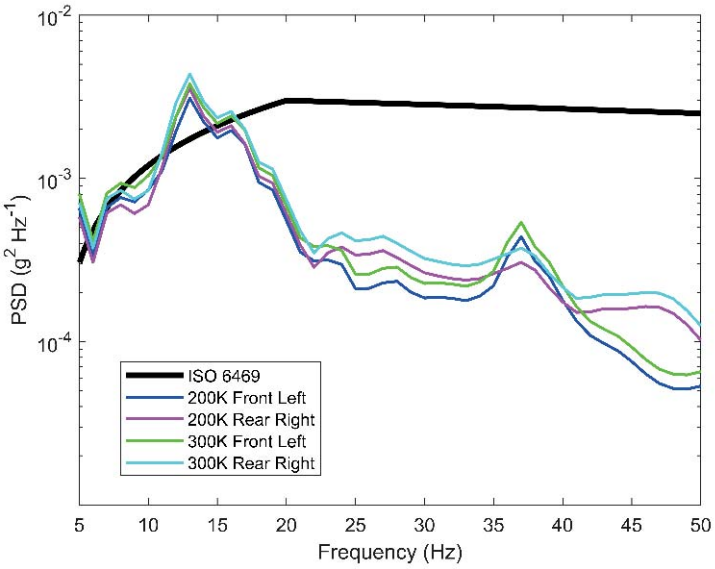

Figure 17: PSD Comparison of ISO and collected data in X-axis

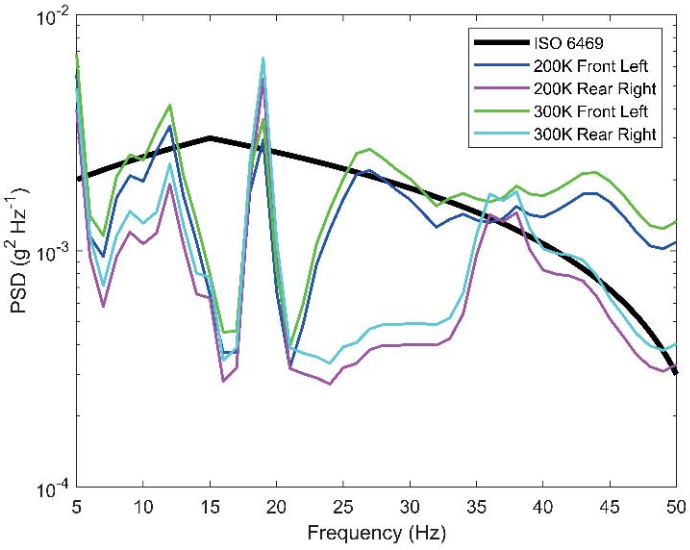

Figure 18: PSD Comparison of ISO and collected data in Y-axis

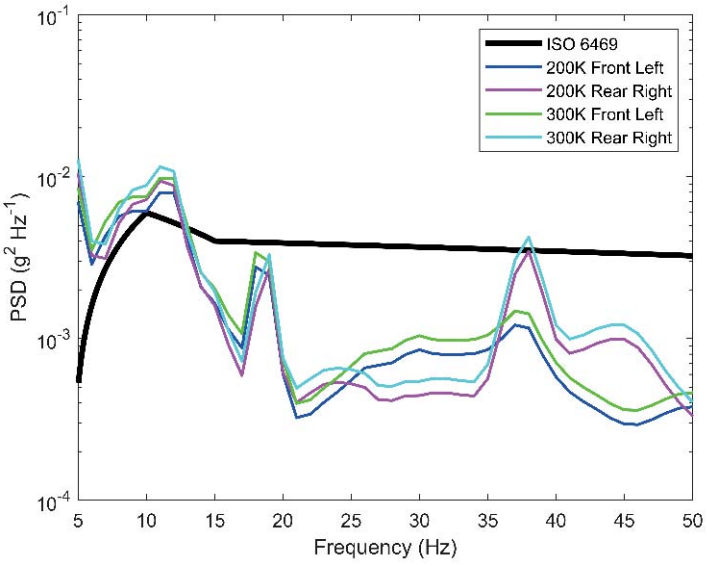

Figure 19: PSD Comparison of ISO and collected data in Z-axis

CHAPTER III

ANALYTICAL VEHICLE MODEL AND DATA

In this chapter, details of a multibody dynamics model are explained in detail. More specifically, subsystem models of the vehicle model and the tire / road models are provided in Section 3.1. Then, correlation of the model to physical testing are given in Section 3.2.

3.1 Analytical Vehicle Model

There has been an increasing trend to use simulation models in the automotive industry [42]. The improved accuracy of these simulation models increase their use in the product development and vehicle sign-off confidently [43]. Since the Computer Aided Engineering CAE tools help the designers improve their design before the physical tests, they are inevitable part of the durability studies.

The determination of the durability road load data of a new vehicle is an important challenge for the CAE teams in OEMs. The CAE teams use simulation tools in order to make design decisions of design parameters such as suspension stiffness, shock absorbers. Since all these parameters affect the road load data and the forces acting on the components, detailed simulation models are needed. The Virtual Proving Ground VPG model is one of the most common simulation models used in the automotive industry today [44],[45],[46]. The virtual iteration method is an alternative approach to VPG models [47]. These simulation tools can calculate loads with high accuracy and confidence provided the correct input parameters are used. The RLD engineers can determine the road loads by replicating the physical tests on the virtual prototype. For this purpose, the multi-body dynamics model MBD of the vehicle, tire model and road model are integrated as part of the overall VPG model, shown in figure 20. The road load data is then

shared with the design teams to support subsequent design iterations to complete the vehicle design that meets customer and regulatory requirements. VPG analyses of the electrical vehicle are performed to extract road loads from the analtical model. The accelerations at different locations of the battery are measured to compare with the test resuts from the prototype vehicle.

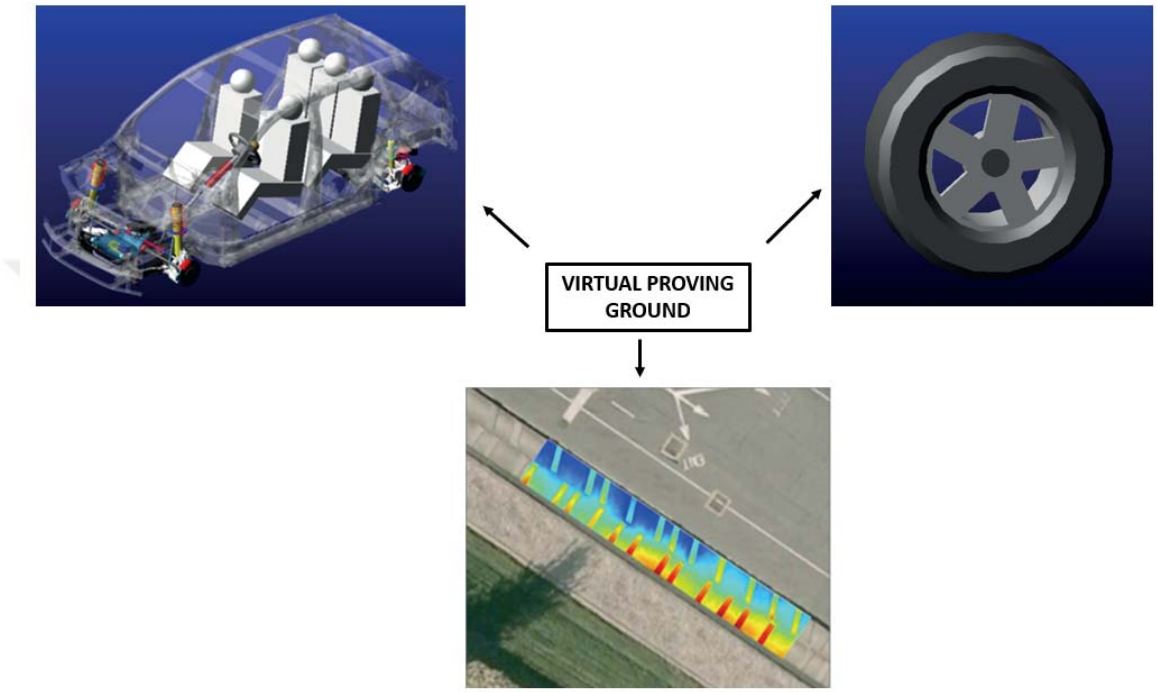

Figure 20: Vehicle, tire and road [48] models

3.1.1 Vehicle Modeling

A vehicle model is created from templates, subsystems and assembly in most of Multibody Dynamics softwares. Assembly is consisting of dynamic systems of the vehicle called subsystems. Templates are the advanced parameter included subsystem elements in the model.

3.1.1.1 Template

Advanced modelling element for common systems is called template in Multibody Dynamics vehicle model in Adams/Car. Templates define the default geometric data, topology of models and parametrically defined components[49]. Templates

are used to advance modelling for details of the system like suspensions, powertrain, tires, rigid or flex body of the vehicles, antiroll bars and steering. In templates, you can model and create hard points, part informations like mass, cog and inertias, axis informations, attachments like joints and bushings, force elements such as springs and dampers and parametrical variables like gear ratios or suspension kinematic variables camber and toe angles. Template builders in MSC Adams is also the place of connection of the different systems and templates to be connected via communicaters. Example of a multilink suspension template from Adams library can be seen in Figure 21.

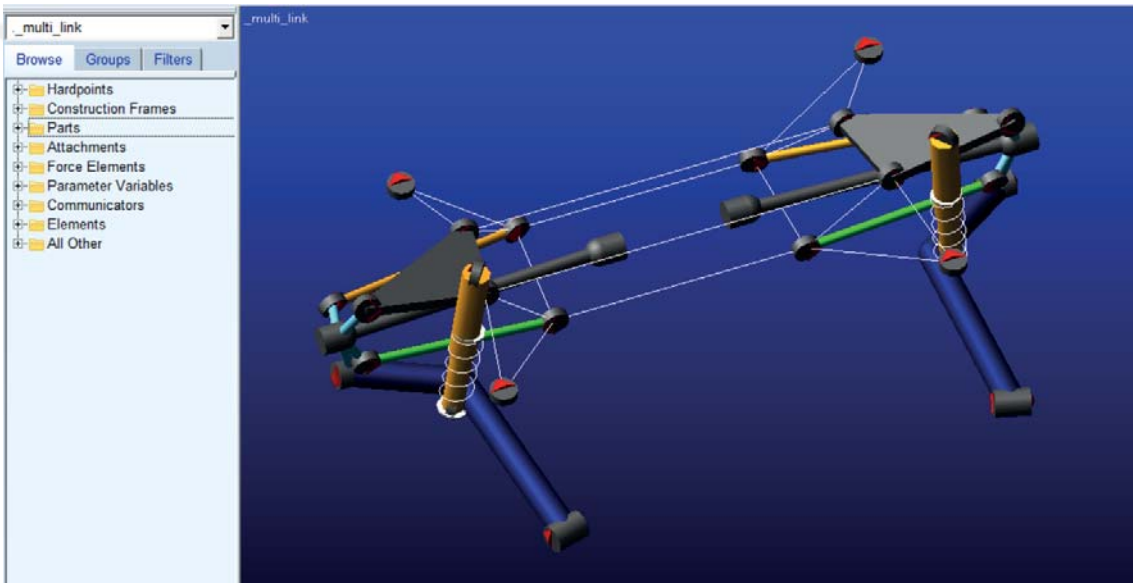

Figure 21: Template example of multilink suspension from Adams shared library

3.1.1.2 Subsystem

Subsystems are template based systems which allow us to change parametric variables in dynamic system within standard interface of MSC.Adams. Subsystems are created with the base of templates. Fundamental changes like communicators or joint elements can not be changed in subsystems. As in the name subsystems are creating the vehicle model with sub-systems of the vehicle. Same template can be used for 2 different subsystem such as front and rear tire subsystem model can be made from same tire template. Hard points, mass and inertia informations,

bushing and spring stiffnesses, damping forces and parametrical variables like gear ratios or suspension kinematic variables camber and toe angles can be updated via subsystems and updated values are taken into account during multibody runs. Example of a multilink suspension subsystem from Adams library can be seen in Figure 22.

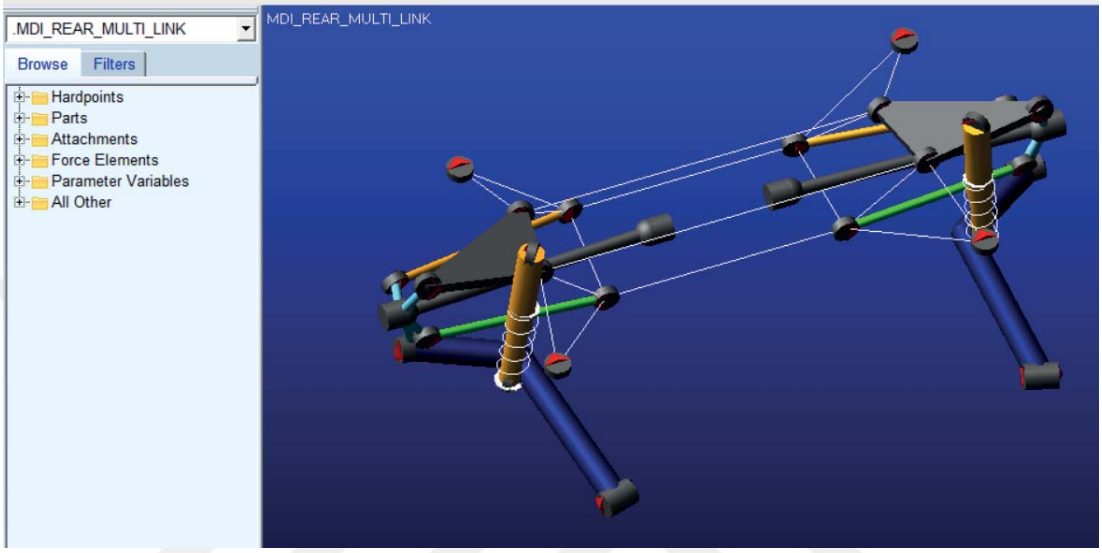

Figure 22: Subsystem example of multilink suspension from Adams shared library

3.1.1.3 Assembly

All the created subsystems in a vehicle model such as suspensions, powertrain, tires, rigid or flex body of the vehicles, antiroll bars and steering are representing the vehicle model under assembly. Subsystems come together to form main vehicle assembly model. All these systems working simultanously and communicating each other during the simulations. Assembly is used to run control model or vehicle in different analysis environment which based on real life vehicle drives or rig tests. Kinematics and Compliance test rig, steering runs for vehicle characteristic determination such as J-turn, swept steers and fish hook, cornering events, different driving conditions like acceleration, braking as well as durability special surface runs can be reproduced in analysis environment with a suitable dynamic assembly (vehicle) model. Example of an assembly from Adams library can be

seen in Figure 23.

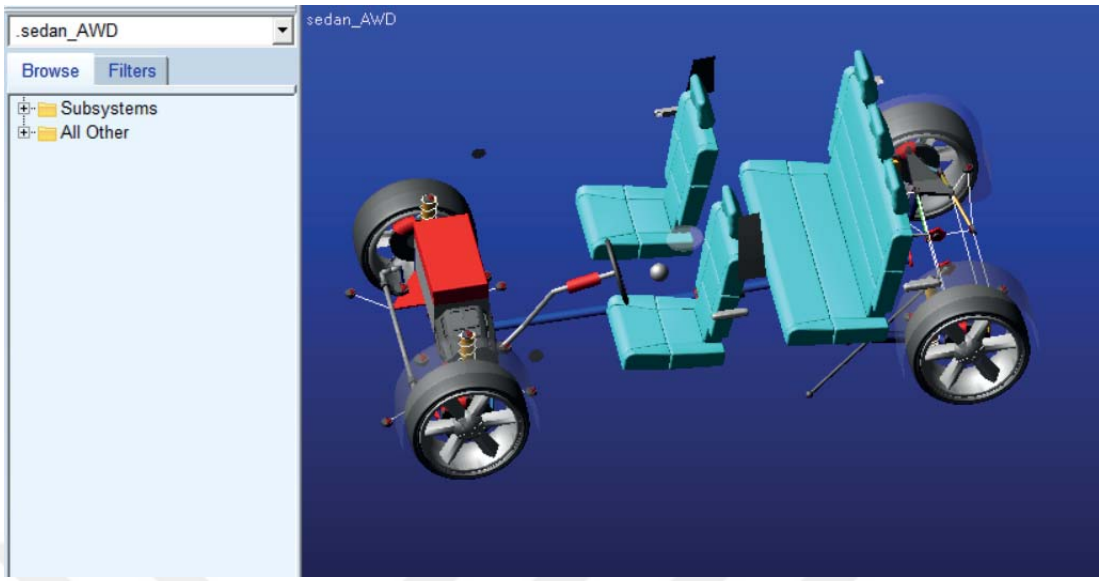

Figure 23: Assembly example of a vehicle model from Adams shared library

3.1.1.4 Rigid and Flex Bodies

Nondeformable bodies are called rigid body. Rigid body is the part which is not deformed under load. It reduces load transfer calculations in the solver. Rigid body assumption is used to reduce modeling and run time and complexity of the model.

Flex bodies are the flexible bodies which can deform under load. Flex body is the elastic representation of the parts. It is a finite element representation. In general conditions, multibody dynamics does not need design(geometry) information of the parts. Parts can be modelled parametricly. But to be able to model a part as a flex body, computer aided design CAD of the part is needed. To create flex body modal neutral file MNF of the part should be created. MNF's are finite element representation of the geometrical information of the parts and it defines flexiblitiy in the Adams. MNF includes the information of;

- Geometry (location of nodes and node connectivity)
- Nodal mass and inertia

- Mode shapes
- Generalized mass and stiffness for mode shapes [50]

In the MNF creation, the boundary points of the joints are assumed fixed and their motion is combined with the modes of the structure [44]. These fixed points are independent from joining type and stores the connection point information. After parametric creation of the part or body in the multibody environment, MNF information can be uploaded to the part and points of the MNF model can be coupled with the hardpoints and joints of the multibody model. During the dynamic simulations, mode shape information is used to identify deformation of the flex body and multibody solver uses displacement information to calculate equation of motion, equation 9.

$$F(t) = m\ddot{x} + c\dot{x} + kx \tag{9}$$

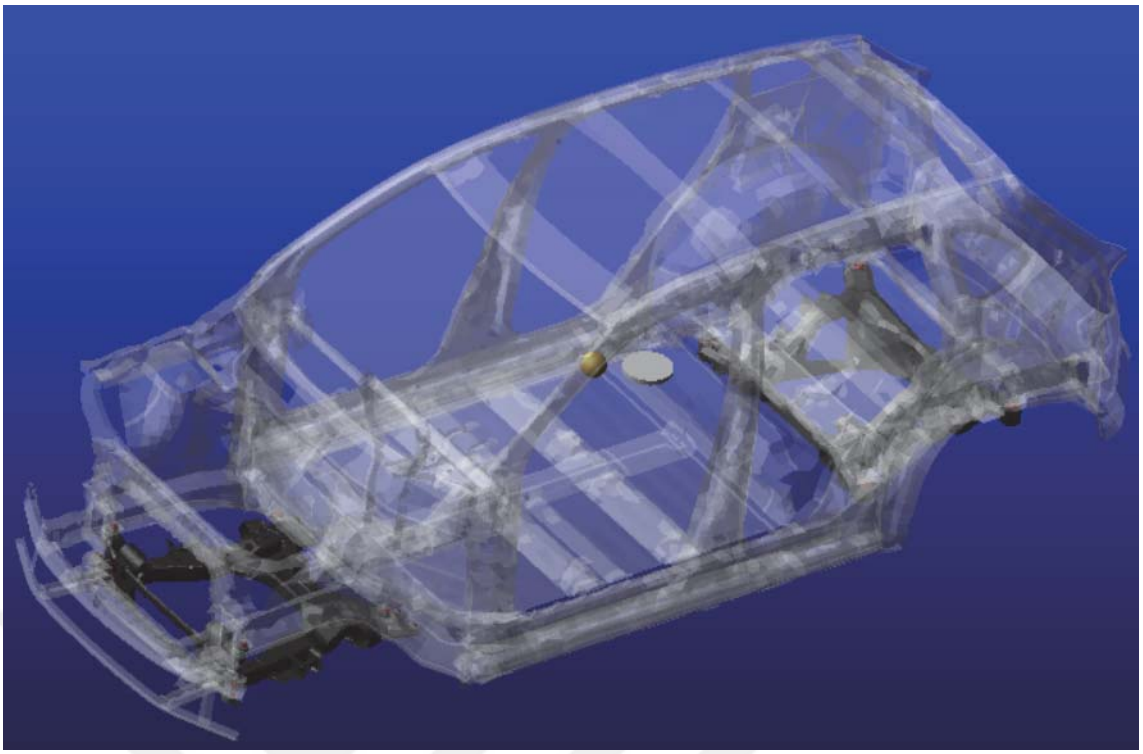

Figure 24: Flexible body of the used vehicle model

3.1.1.5 Vehicle Model

Vehicle is built in Adams environment as templates, subsystems and final assembly. In the multibody dynamic models the parts are modelled as rigid and flexible models. The joints are used to constraint the motion of the parts. The results are determined in the form of the accelerations, and forces. The VPG model is based on the MSC Adams. In the vehicle model, there are two electric motors at the front and rear axles with the relevant parameters. Final drive ratio is defined as the overall gear transmission ratio. Most of the chassis components like subframes, links and LCAs are modelled as flexible models. For this purpose, the finite element models are developed, and the modal analysis are performed to get MNF represantations. These results are converted to modal models and integrated to the MBD model. The bushings are modelled as linear translational and rotational springs in longitudinal, lateral and vertical directions. The dynamic effects of the forces are taken into account using scale factors. Static force displacement

relationship for lower control arm bushing is shown in Figure 25. Anti-roll bars are modelled using beam elements to consider their flexibility.

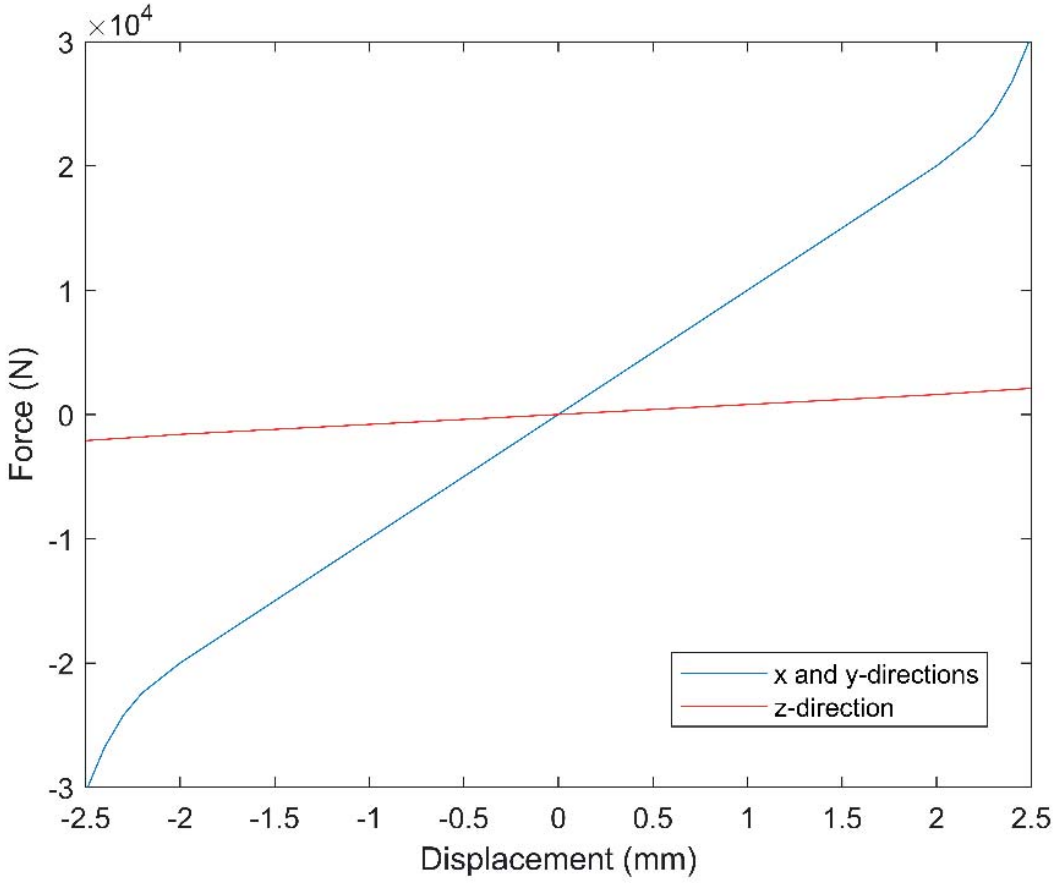

Figure 25: Bushing force at lower control arm

Finally, the body-in-white (BIW) of the vehicle is modelled as flexible model. The battery model, shown in Figure 26, is implemented into the body in white (BIW) model. The finite element representation of the battery for multibody model is calculated with BIW. Joints between BIW and battery are modelled as beam elements. MNF file is created with overall finite element model of BIW with battery.

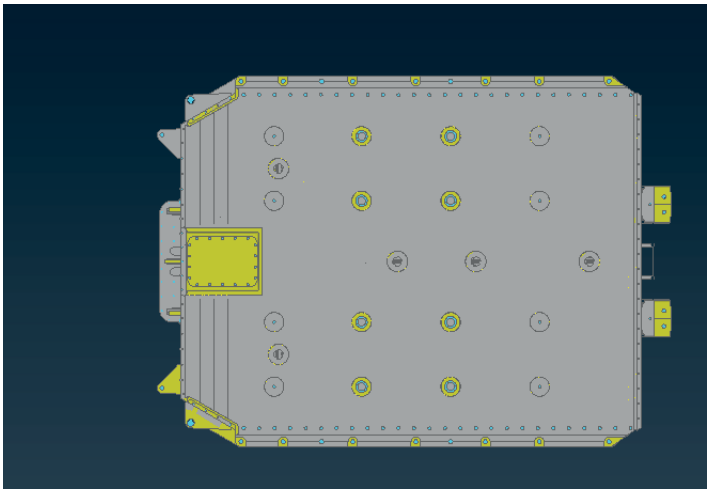

Figure 26: The FEA model of the battery

The full vehicle model, shown in Figure 27, has 2188 degrees of freedom (DOFs) and 213 moving parts.

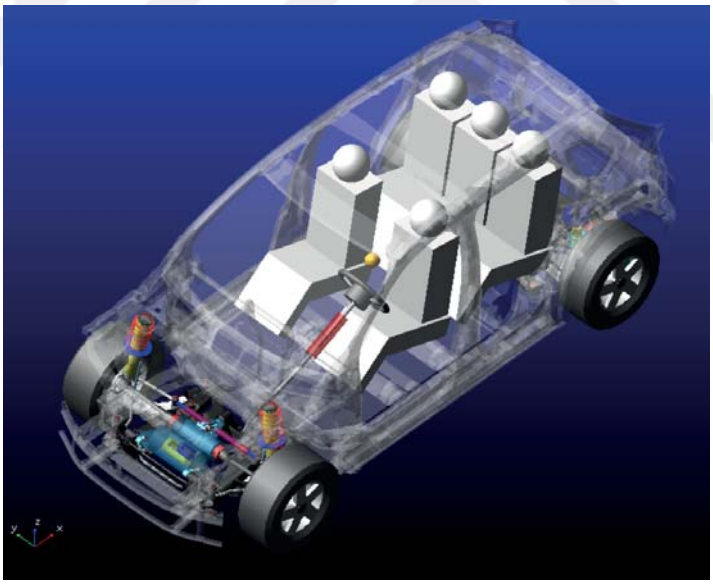

Figure 27: Full vehicle model used in VPG Simulations

3.1.2 Tire Model

Since the effect of tire models on vehicle dynamics is significant, the tire model should also include frequency dependence. For this purpose, FTire model is used to realistically model the interaction between road and the tire. FTire model is

a nonlinear model for accurate simulation of ride comfort and shock events for high frequencies. The model is a structural dynamics based model, where the rim model is flexible and the tire belt is represented as a flexible ring [51]. The parameters of the tire model are derived from static and dynamic testing. Another advantage of the FTire model is that it is computationally efficient [51].

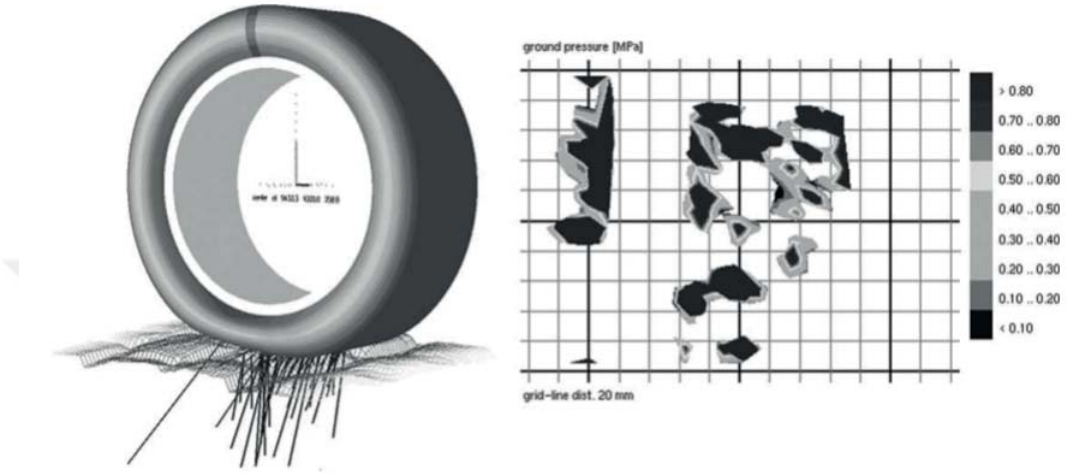

Figure 28: Pressure profile of the Ftire model on Belgian block road [51]

3.1.3 Road Model

Roads are important elements of the VPG model to represent the interaction between the tires. Regular roads such as potholes, and chuckholes can be easily represented in the VPG model. However, the representation of the irregular roads such as the cobblestone and Belgian pave require the scanning of the ground surfaces. For that purpose regular and irregular roads can be scanned with external scanning devices and the road surfaces can be formatted digitally in openCRG 3D. Typically grid sizes of openCRG roads are less than 1 cm $\times$ 1 cm [46]. In Figure 29 curved reference line describes the random closest point to the road center which includes road information such as elevation, declination, and slope ([44], [45]). The tire model needs to evaluate the road surface at arbitrary x, y positions during the vehicle simulations, which requires interpolation between measured road data points [45].

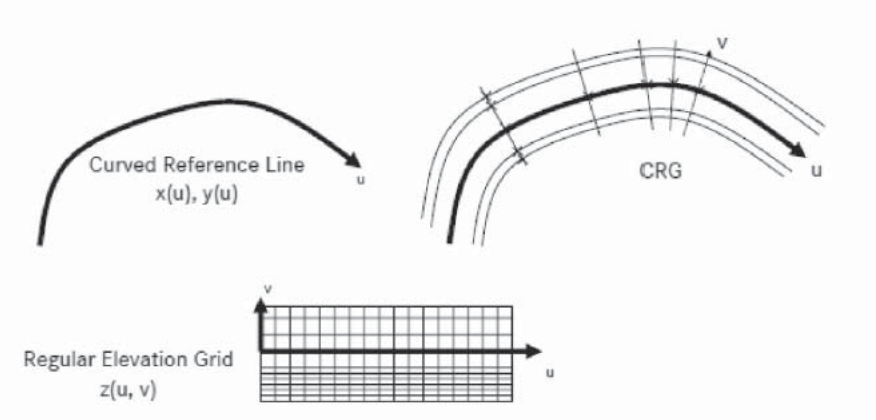

Figure 29: Concept of the OpenCRG road model [45]

The physcial durability test on proving grounds can be performed on analytical environment with multibody dynamics vehicle model and measured tire model by scanning of the road surfaces. There are couple of proving grounds roads avaliable commercially. These scanned roads can be purchased from service suppliers. In Europa the well-known proving grounds such as Idiada (figure 30) and Mira (figure 31) have their proving ground scanned and they are commercially avaliable in the market for virtual proving ground analysis.

Figure 30: Pave road example from Idiada Proving Ground [52]

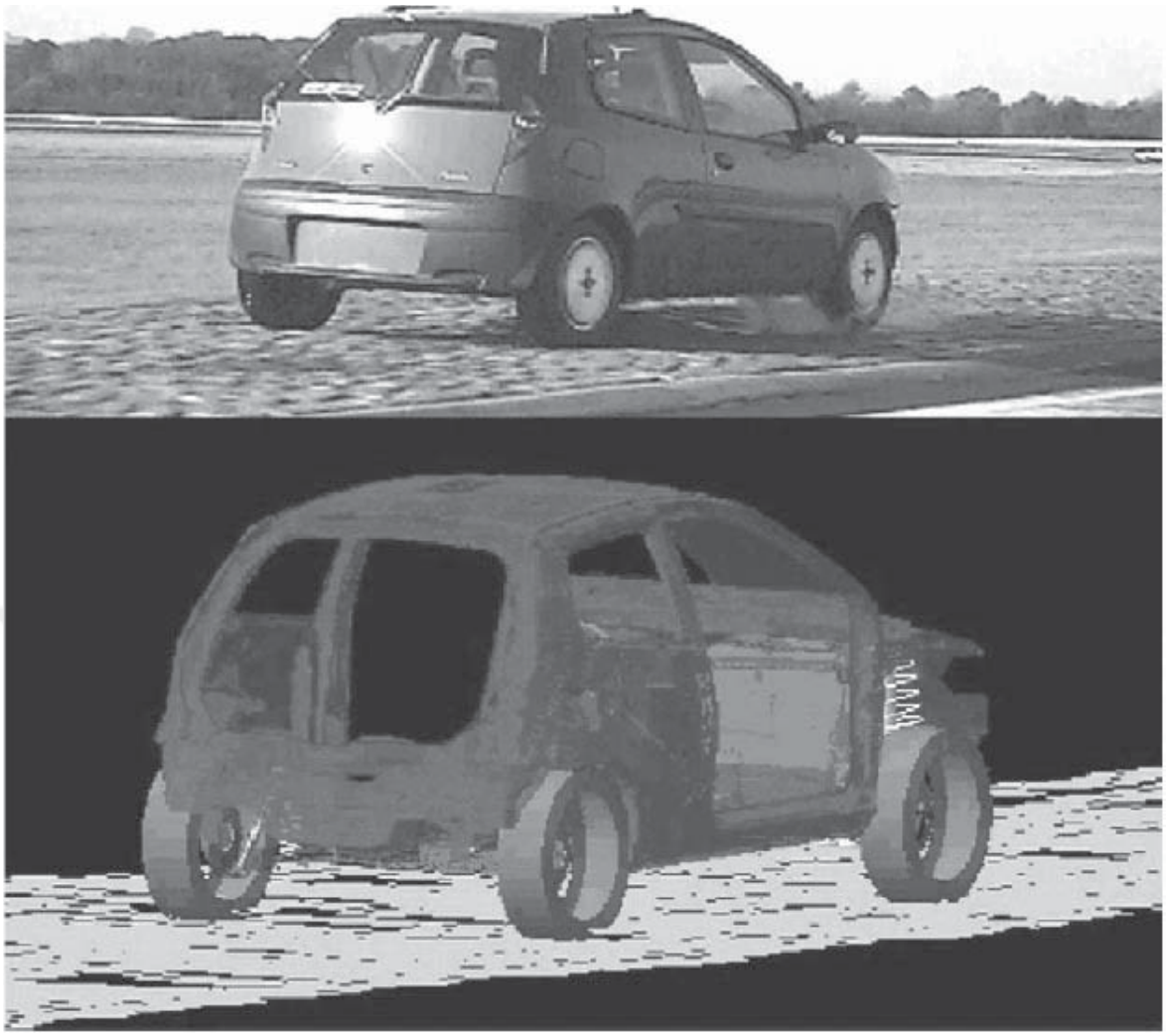

Figure 31: Pave road example from Mira Proving Ground [53]

3.2 Correlation and Results

The VPG model including the FTire model is simulated using the proving ground test procedure to extract road loads as in the physical test procedure. The acceleration of the battery is extracted from flexible model of battery. Road load data is processed similar to the processing of the experimental data. Finally, overall FDS profiles from VPG model and experimental data are compared. The FDS comparison results are shown in Figure 29, Figure 30, and Figure 31 for x, y and z directions, respectively.

The FDS results of Z direction show that VPG loads are higher than physically collected data. This situation is due to the fact that the battery in the prototype vehicle is not fully representative and smaller than the designed battery for the vehicle. Only in Y direction, collected data is higher than the analytical loads because prototype battery is shorter in Y direction. Beside this results, centre data is also smaller than the corner accelerometers data for both collected and analytical data. This shows in both analytical and physical vehicle transfer of the loads from corners to the center is low. As a result center data has lower fatigue content.

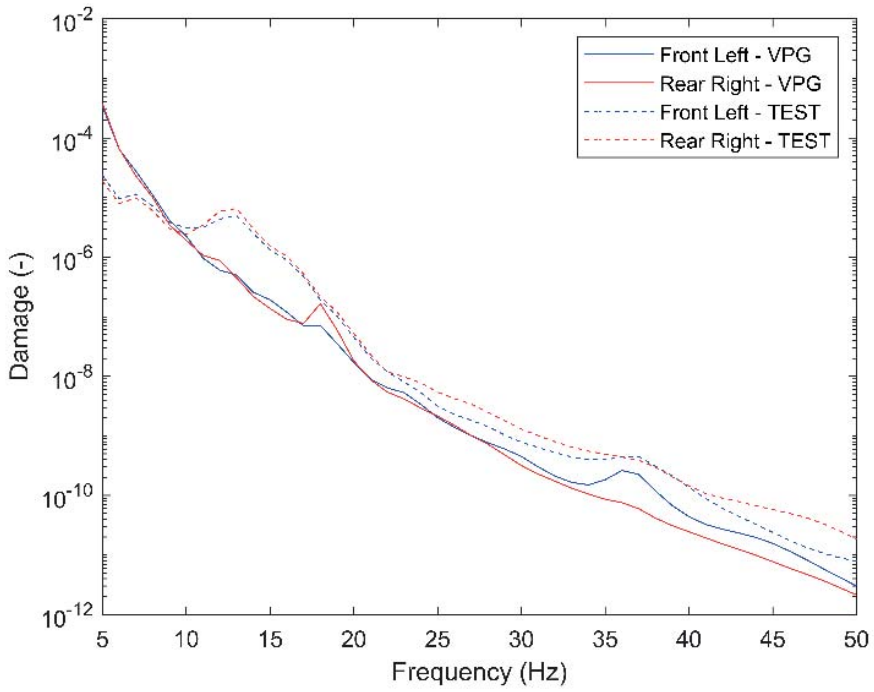

Figure 32: FDS Comparison of VPG and collected data in X-axis

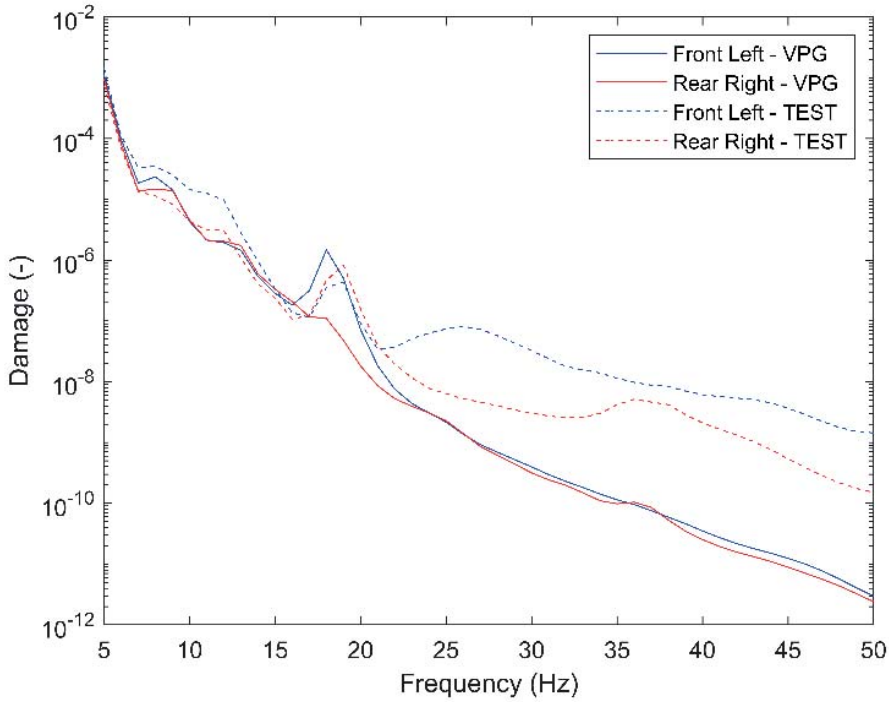

Figure 33: FDS Comparison of VPG and collected data in Y-axis

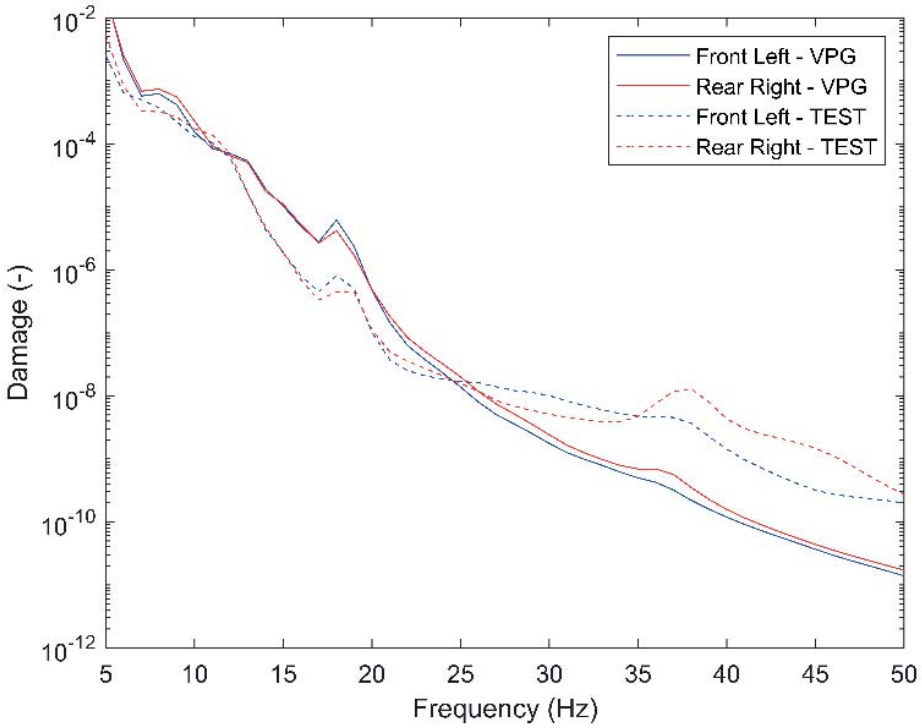

Figure 34: FDS Comparison of VPG and collected data in Z-axis

CHAPTER IV

CONCLUSION

The determination of efficient and accurate representation of durability testing may positively affect the overall vehicle design such as lightweight and fuel efficient vehicles. The structural life of the battery is investigated in this study. In this paper, test data collected from a C-SUV class vehicle is used to compare the most commonly used standards for 200K and 300K lifecycles with the global proving ground endurance procedure. Simultaneously, simulations based on multibody dynamics are compared with experimental data.

The results show that different vehicle and different durability procedures have variations compared to the standards. The findings from this study show that the ISO-6469-1 standard does not cover the life expectancy of the battery system. The results also show that the variation of the loads in different directions such as longitudinal and lateral directions should be taken into account. Since the experimental data have fatigue loads in the 5-10 Hz frequency range, these frequencies should be taken into account when creating the test profile.

The simulation tools are increasingly used in the automotive industry. The results from this study reveal that collected vehicle data and VPG model show a high correlation. While the collected data is always preferrable to determine the battery life cycle, given the high correlation levels, VPG results can be alternatively used as battery durability test PSD profile for shaker tables. The findings from the paper serve as general guidelines to determine the durability testing of the battery of electric vehicles.

CHAPTER V

FUTURE WORK

The studies carried out in this thesis will lead to future studies in this field. VPG analysis is powerfull solution to be able to determine vehicle road loads coming from the road surfaces. Possible future research topics are:

- Vibrational fatigue tests and performances of the battery modules and cells can be investigated as well as battery pack.
- VPG analysis can be used to exract road loads for various points on the vehicle such as suspension, chassis, body, interior or exterior components. Extracted data either can be used for durability CAE analysis or test data creations of the components instead of standards.
- Performance evaluations of the all vehicle system on harsh roads can be performed such as antipinching system of the windows.
- Beside durability advanced driver assistance systems also can be evaluated in virtual environment.

Bibliography

[1] S. Amjad, S. Neelakrishnan, and R. Rudramoorthy, "Review of design considerations and technological challenges for successful development and deployment of plug-in hybrid electric vehicles," *Renewable and Sustainable Energy Reviews*, vol. 14, no. 3, pp. 1104–1110, 2010.

[2] C. Yap, "Honda aims to find a 'second life' for hybrid/ev battery packs." https://www.piston.my/2020/04/17/honda-aims-to-find-a-second-life-for-hybridev-battery-packs/. (accessed: 01.04.2022).

[3] D. Nagra, "Electric car battery life how concerned should you be about degradation." https://www.which.co.uk/news/2020/10/electric-car-battery-life-how-concerned-should-you-be-about-degradation/. (accessed: 01.04.2022).

[4] A. Kampker and et al., "Evaluation of a remanufacturing for lithium ion batteries from electric cars," *International Journal of Mechanical and Mechatronics Engineering*, vol. 10, no. 12, pp. 1929–1935, 2016.

[5] N. Lutsey and M. Nicholas, "Update on electric vehicle costs in the united states through 2030," *The International Council on Clean Transportation*, vol. 196, no. 23, pp. 10351–10358, 2019.

[6] M. Wang, F. Jiang, Q. Zhang, and S. Song, "Matching up the suspension of electric vehicle with the supporting system of battery pack," *Mechanika*, vol. 20, no. 4, pp. 402–406, 2014.

[7] "Electrically propelled road vehicles test specification for lithium-ion traction battery packs and systems part 2: High-energy applications," standard, International Organization for Standardization, July 2012.

[8] "Electrically propelled road vehicles, safety specifications, part 1: Rechargeable energy storage system (ress)," standard, International Organization for Standardization, Apr. 2019.

[9] "Ak-lh 5.21 : Betriebsfestigkeit elektromobilität," ak-lh standard, 2011.

[10] "Vibration testing of electric vehicle batteries," standard, Society of Automotive Engineers, Dec. 2013.

[11] J. M. Hooper and J. Marco, "Characterizing the in-vehicle vibration inputs to the high voltage battery of an electric vehicle," *Journal of Power Sources*, vol. 245, pp. 510–519, 2014.

[12] G. Kjell and J. F. Lang, "Comparing different vibration tests proposed for li-ion batteries with vibration measurement in an electric vehicle," tech. rep., World Electric Vehicle Symposium and Exhibition (ESV27), Barcelona, Spain, Nov. 2013.

[13] J. Hooper and J. Marco, "Defining a representative vibration durability test for electric vehicle (ev) rechargeable energy storage systems (ress)," *World Electric Vehicle Journal*, no. 2, pp. 327–338, 2016.

[14] J. Hooper and J. Marco, "Understanding vibration frequencies experienced by electric vehicle batteries," (London, England), pp. 1–6, Hybrid and Electric Vehicles Conference, IET, Nov. 2013.

[15] J. Hooper, J. Marco, G. H. Chouchelamane, J. S. Chevalier, and D. Williams, "Multi-axis vibration durability testing of lithium ion 18650 nca cylindrical cells," *Journal of Energy Storage*, vol. 15, pp. 103–123, 2018.

[16] A. Halfpenny and M. Pompetzki, "Proving ground optimization and damage correlation with customer usage," *SAE International Journal of Materials and Manufacturing*, vol. 4, no. 1, pp. 620–631, 2011.

[17] C. Garcia, J. Aran, and S. Ruiz, "Design of reliable accelerated fatigue test programs based on real market use," *SAE Technical Paper*, 2010.

[18] A. Londhe, S. Kangde, and K. Karthikeyan, "Deriving the compressed accelerated test cycle from measured road load data," *SAE Technical Paper*, 2012.

[19] "Vibration testing of electric vehicle batteries," standard, United States Department of Energy, Washington DC, USA, Jan. 1996.

[20] P. K. Tripathi and N. Kumar, "Fatigue damage spectrum-based assessment of vibration standards on battery pack for ev's using stress as a response metric," (Bengaluru, India), 2019 IEEE Transportation Electrification Conference (ITEC-India), IEEE, Dec. 2019.

[21] "Secondary lithium-ion cells for the propulsion of electric road vehicles – part 2: Reliability and abuse testing," standard, International Electrotechnical Commission, Dec. 2018.

[22] M. A. Biot, "Theory of elastic systems vibrating under transient impulse, with an application to earthquake-proof buildings," *Proceedings of the National Academy of Science of the United States of America*, vol. 19, no. 2, pp. 262–268, 1933.

[23] C. Lalanne, *Mechanical Vibration and Shock Volume 2, Second Edition*. Hoboken NJ, USA: John Wiley Sons Inc., 2002.

[24] A. Halfpenny, "Accelerated vibration testing based on fatigue damage spectra," *nCode International*, 2006.

[25] A. Halfpenny and T. C. Walton, "New techniques for vibration qualification of vibrating equipment on aircraft," *nCode International*, 2010.

[26] A. Halfpenny, "Methods for accelerating dynamic durability tests," (Southampton, UK), pp. 17–19, Proc. of the 9th International Conference on Recent Advances in Structural Dynamics, 2006.

[27] J. W. Miles, "On structural fatigue under random loading," *Journal of the Aeronautical Sciences*, vol. 21, no. 11, pp. 753–762, 1954.

[28] C. Lalanne, *Vibrations et chocs mécaniques - Tome 3, Vibrations aléatoires*. Paris, France: Hermes Science Publications, 1999.

[29] I. Matsuishi and T.Endo, "Fatigue of metals subjected to varying stress," tech. rep., Presented at Japanese Society of Mechanical Engineers, Fukuoka, Japan, 1968.

[30] S. A. Downing and D. F. Socie, "Simple rainflow counting algorithms," *International Journal of Fatigue*, no. 4, pp. 31–40, 1982.

[31] Y. Lee and T. Tjhung, *Rainflow Cycle Counting Techniques, Metal Fatigue Analysis Handbook*. Butterworth-Heinemann, 2012.

[32] W. Schutz, *A history of fatigue, Engineering Fracture Mechanics*, vol. 54(2). 1996.

[33] A. Wöhler, "Versuche zur ermittlung der auf die eisenbahnwagenachsen einwirkenden kräfte und die widerstandsf ähigkeit der wagen-achsen," *Zeitschrift für Bauwesen*, pp. 583–616, 1860.

[34] O. H. Basquin, "The exponential law of endurance test," *Proceedings of the American Society for Testing and Materials*, vol. 10, pp. 625–630, 1910.

[35] B. P. Allen, "Brittlealuminium320mpa s-n curve." https://en.wikipedia.org/wiki/August-Wöhler. (accessed: 01.04.2022).

[36] M. A. Miner, "Cumulative damage in fatigue," *Journal of Applied Mechanics, ASME 12*, pp. 159–164, 1945.

[37] C. Lalanne, *Mechanical Vibration and Shock: Fatigue Damage, third edition*. Hoboken NJ, USA: John Willy and Sons Inc., 2014.

[38] C. Lalanne, *Mechanical environment test specification development method, third edition*. Le Barp, France: Scientific and Technical Studies Center of Aquitaine, 1997.

[39] H. Mira, "Proving ground surfaces." https://www.horiba-mira.com/Proving-Ground/proving-ground-surfaces/. (accessed: 01.04.2022).

[40] C. Dun, G. Horton, and S. Kollamthodi, "Improvements to the definition of lifetime mileage of light duty vehicles," *Ricardo-AEA*, 2015.

[41] J. Zheng and et al., "Survival rate of china passenger vehicles: a data-driven approach," *Energy Policy*, vol. 129, pp. 587–597, 2019.

[42] O. Tuncel, P. Sendur, M. Ozkan, and A. Guney, "Ride comfort optimisation of ford cargo truck cabin," *International Journal of Vehicle Design*, vol. 52, no. 1-4, pp. 222–236, 2010.

[43] P. Sendur, B. Ozan, M. E. Uyanık, Y. Oz, and S. I. Yılmaz, "A model validation methodology for evaluating rollover resistance performance of a ford commercial vehicle," *SAE Technical Paper*, 2010.

[44] D. Y. M. Reddy and S. Padmanabhan, "Virtual full vehicle durability testing of a passenger car, m.sc. thesis," tech. rep., Department of Applied Mechanics, Chalmers University of Technology, Goteborg, Sweden, 2017.

[45] A. Schmeitz and W. Versteden, "Road load simulation using the mf-swift tire and opencrg road model," *SAE Technical Paper*, 2011.

[46] A. Tang, N. Tamini, and D. Yang, "Virtual proving ground–a cae tool for automotive durability, ride and handling and nvh applications," (Detroit, USA), Proc. of the 6th International LS-DYNA Users Conference, 2000.

[47] A. Vemuri, N. Talekar, and B. Avutapalli, "Road loads for durability analysis using virtual iterations," *SAE Technical Paper*, 2018.

[48] Mscsoftware, "Adams encvpg for horiba mira virtual proving ground." http://www.mscsoftware.com/sites/default/files/TK-Adams-EncVPG-LTR-w.pdf. (accessed: 01.04.2022).

[49] U. Author, "Templates," *MSC Adams 2020 Online Help*, 2020.

[50] U. Author, "Modal neutral file (mnf)," *MSC Adams 2020 Online Help*, 2020.

[51] M. Gipser, "Ftire–the tire simulation model for all applications related to vehicle dynamics," *Vehicle System Dynamics*, vol. 45, no. S1, pp. 139–151, 2007.

[52] J. Arbiol, J. A. Muñoz, X. Armengo, and E. Aramburu, "Full vehicle durability analysis by means of the idiada virtual proving ground," in *Proceedings of the FISITA 2012 World Automotive Congress*, (China), pp. 337–347, 2012.

[53] D. Ensor, C. Cook, and M. Birtles, "Optimising simulation and test techniques for efficient vehicle durability design and development," *SAE Technical Paper*, 2005.

VITA

Halil Zınar Düzgün graduated from Hacettepe University with an Automotive Engineering degree in 2016. After graduation, he worked for S-T Engineering, Ford Otosan A.Ş. and TOGG. His main area of research interest is on Durability Road Load Data Engineering. He is proficient with Multibody Dynamic analysis like Virtual Proving Ground Analysis and Time Waveform Replication Analysis for heavy commercial vehicles and passenger cars. Besides, he has been involved with road load data collection, where he created different durability test profiles like electromechanical shakers and hydraulic test systems for different types of vehicle projects. Furthermore, he also has experience on customer correlation studies for vehicle level durability tests.